Journal of Hydrology 388 (2010) 438–455

Contents lists available at ScienceDirect

Journal of Hydrology

journal homepage: www.elsevier.com/locate/jhydrol

Soil–Litter–Iso: A one-dimensional model for coupled transport of heat, water and stable isotopes in soil with a litter layer and root extraction

Vanessa Haverd [a,*], Matthias Cuntz [b,1]

[a] CSIRO Marine and Atmospheric Research, GPO Box 3023, Canberra ACT 2601, Australia
[b] Max-Planck-Institut für Biogeochemie, Hans-Knöll-Str. 10, 07745 Jena, Germany

ARTICLE INFO

Article history:
Received 30 September 2009
Received in revised form 23 April 2010
Accepted 15 May 2010

This manuscript was handled by Andras Bardossy, Editor-in-Chief, with the assistance of Ehab Erwin Zehe, Associate Editor

Keywords:
Coupled heat and water transport
Water isotopes
Litter
Evapotranspiration
Soil moisture
Land surface model

SUMMARY

We present a new isotopically enabled hydrologic scheme, "Soil–Litter–Iso", suitable for use as part of an isotopically enabled land surface model. Soil–Litter–Iso is a one-dimensional model for coupled transport of heat, water and stable isotopes (HDO and $H_2{}^{18}O$) in soil and litter. It is sufficiently efficient for use at regional scale, yet includes the complexity of coupled heat and water transport enabling decomposition of the total moisture flux into liquid and vapour components. The numerical implementation is based on Ross' fast solution to the Richards equation (Ross, 2003). This, combined with the explicit solution of the energy and moisture equations at the soil/air interface, permit the isotopic calculations to be performed with thick soil layers and large times steps, resulting in significantly improved computational efficiency compared with existing isotopically-enabled soil models of similar complexity. We demonstrate the model's numerical accuracy by conducting a series of established test-cases and comparing predictions of steady-state isotopic concentration profiles with corresponding analytical solutions. We also demonstrate the model's operation within a land surface model by performing simulations for the forested flux site at Tumbarumba in south-eastern Australia. These simulations show that the total evapotranspiration (ET) flux, its components and their isotopic signatures are very sensitive to the inclusion of litter, and that the model is a useful tool for assessing when the isotopic signatures of the ET components are sufficiently distinct to be useful for flux partitioning.

1. Introduction

An isotopically enabled hydrologic model is used to estimate soil moisture stores and fluxes (soil evaporation; root extraction; deep soil drainage and surface runoff), as well as the associated concentrations of minor water isotopologues (HDO and $H_2{}^{18}O$). It is an essential component of an isotopically enabled land surface scheme (LSM) that is part of an atmospheric circulation model. Isotopically enabled models of the atmosphere, hydrology and the biosphere are used in a variety of applications, which include separation of evapotranspiration into evaporation from the soil and transpiration from the plants (e.g. Ferretti et al., 2003), tracing water movement within the soil-vegetation-atmosphere system (e.g. Fekete et al., 2006), and partitioning terrestrial CO_2 fluxes between photosynthesis and respiration using $\delta^{18}O$ in atmospheric CO_2 (e.g. Ogée et al., 2004). Water isotopes are also important for paleoclimate research either directly through the stable isotopic composition of ice cores (Jouzel et al., 2007) or indirectly, for example through their imprint on the isotopic composition of molecular oxygen, the Dole effect (Dole et al., 1954; Hoffmann et al., 2004).

To date, the state-of-the-art model for the coupled transport of heat, water and stable isotopes in bare soil is SiSPAT-Isotope (Braud et al., 2005a) It builds on earlier isotopically-enabled soil models of Shurbaji and Phillips (1995), Melayah et al. (1996) and Mathieu and Bariac (1996). All of these are based on the one-dimensional coupled transport of heat and water in soil (Philip, 1957), which permits the total moisture flux to be separated into liquid-phase and vapour-phase components. SiSPAT-Isotope is shown to accurately reproduce analytical solutions for the steady-state vertical isotopic profiles in saturated and unsaturated soils (Barnes and Allison, 1983; Barnes and Allison, 1984). It also shows reasonable agreement with laboratory data sets (Braud et al., 2009a, 2005b, 2009b). Despite these successes, the application of SiSPAT-Isotope has not been extended either to vegetated field sites or to regional scale. A likely reason for this is its lack of numerical efficiency, with soil layer thicknesses of 10^{-6}–10^{-4} m near the surface and time-steps <50 s (Braud et al., 2005a).

* Corresponding author. Tel.: +61 2 6246 5981; fax: +61 2 6246 5988.
E-mail address: Vanessa.Haverd@csiro.au (V. Haverd).
[1] Present address: UFZ – Helmholtz Centre for Environmental Research, Permoserstr. 15, 04318 Leipzig, Germany.

0022-1694/$ - see front matter Crown Copyright © 2010 Published by Elsevier B.V. All rights reserved.
doi:10.1016/j.jhydrol.2010.05.029

Nomenclature

c_{soil}	volumetric heat capacity of soil (J m^{-3} K^{-1})
c_w	volumetric heat capacity of liquid water (J m^{-3} K^{-1})
c_p	volumetric heat capacity of air at constant pressure (J m^{-3} K^{-1})
c_l^i	concentration of minor isotopologue in liquid soil water (kg m^{-3} $H_2O_{(l)}$)
$c_{l,s}^i$	concentration of minor isotopologue in liquid water at the surface (kg m^{-3} $H_2O_{(l)}$)
$c_{l,L}^i$	concentration of minor isotopologue in litter moisture (kg m^{-3} $H_2O_{(l)}$)
$c_{l,0}^i$	concentration of minor isotopologue in pond water (kg m^{-3} $H_2O_{(l)}$)
c_v	concentration of water vapour in soil air spaces (m^3 $H_2O_{(l)}$ m^{-3} (air))
$c_{v,sat}$	saturated concentration of water vapour in soil air spaces (m^3 $H_2O_{(l)}$ m^{-3} (air))
$c_{v,a}$	concentration of atmospheric water vapour (m^3 $H_2O_{(l)}$ m^{-3} (air))
$c_{v,L}$	concentration of water vapour in litter air spaces (m^3 $H_2O_{(l)}$ m^{-3} (air))
$c_{v,s}$	concentration of water vapour at the soil surface (m^3 $H_2O_{(l)}$ m^{-3} (air))
dx	soil layer thickness (m)
dx_L	litter layer thickness (m)
D_l^i	diffusivity of minor isotopologue in liquid water (m^2 s^{-1})
D_v^i	diffusivity of minor isotopologue vapour in the bulk soil (m^2 s^{-1})
D_v	diffusivity of water vapour in the bulk soil (m^2 s^{-1})
$D_{v,a}$	diffusivity of water vapour in air (m^2 s^{-1})
$D_{v,L}$	diffusivity of water vapour in litter (m^2 s^{-1})
$f(\ )$	response function of stomatal conductance to soil moisture
g	gravitational constant (m s^{-2})
$g(\ )$	root density distribution function
G	heat flux into surface (soil or litter) (W m^{-2})
h	pressure head (m)
h_e	pressure head at air entry (m)
h_P	pond height (m)
h_r	relative humidity
$h_{r,s}$	relative humidity at air/soil or air/litter interface
$h_{r,SL}$	relative humidity at litter/soil interface
H	sensible heat flux at soil surface (W m^{-2})
k_H	thermal conductivity of bulk soil (W m^{-1} K^{-1})
k_E	latent heat conductivity of bulk soil (W m^{-1} K^{-1})
K	hydraulic conductivity (m s^{-1})
K_{sat}	hydraulic conductivity (m s^{-1}) of saturated soil
M_w	molar mass of water (kg mol^{-1})
M_i	molar mass of minor isotopologue (kg mol^{-1})
q_{evap}	evaporative flux from soil or litter surface to atmosphere (m s^{-1})
$q_{evap,L}$	evaporative flux from litter/soil interface to litter (m s^{-1})
q_d	drainage flux of liquid water from litter layer to soil column (m s^{-1})
q_H	vertical heat flux (J m^{-2} s^{-1}) within soil column
$q_{H,0}$	vertical heat flux (J m^{-2} s^{-1}) into top of soil column
q_l	liquid-phase flux of soil moisture (m s^{-1})
q_l^i	liquid-phase flux of minor isotopologue (kg m^{-2} s^{-1})
q_v	vapour-phase flux of soil moisture (m s^{-1})
$q_{v,h}$	component of vapour-phase flux of soil moisture (m s^{-1}) due to gradient in h
$q_{v,T}$	component of vapour-phase flux of soil moisture (m s^{-1}) due to gradient in T
q_v^i	vapour-phase flux of minor isotopologue (kg m^{-2} s^{-1})
q_w	flux of soil water (m s^{-1})
$q_{w,0}$	flux of water into top of soil column (m s^{-1})
r_{ex}	sink term accounting for root extraction (s^{-1})
r_{bw}	boundary-layer resistance to water vapour transfer (m^{-1} s)
r_{bH}	boundary-layer resistance to heat transfer (m^{-1} s)
R	gas constant (J mol^{-1} K^{-1})
R_{net}	net radiation absorbed by soil (W m^{-2} s^{-1})
s	$dc_{v,sat}/dT$ (m^3 $H_2O_{(l)}$ m^{-3} (air) K^{-1})
S	degree of effective saturation
T	soil temperature (°C)
T_a	air temperature (°C)
T_L	litter temperature (°C)
T_P	pond temperature (°C)
T_{SL}	temperature at litter/soil interface (°C)
T_s	temperature at air/soil or air/litter interface (°C)
z	vertical co-ordinate (m)
α	root efficiency function
α^+	isotopic equilibrium fractionation factor (<1)
$\alpha_{k,diff}$	ratio of vapour-phase diffusion coefficients (D_v^i/D_v)
α_k	isotopic kinetic fractionation factor (<1)
γ	shape parameter in root efficiency function
η	shape parameter for hydraulic conductivity curve
η_E	enhancement factor for transport of water vapour across a temperature gradient
λ	shape parameter for soil moisture retention curve
λ_L	shape parameter for litter moisture retention curve
λ_E	latent heat of vaporisation (J kg^{-1})
$\lambda_E E$	latent heat flux at surface (W m^{-2})
ϕ_l	liquid matric flux potential (m^2 s^{-1})
ρ	density of liquid water (kg m^{-3})
	density of air
ρ_b	dry bulk density of soil
$\rho_{b,L}$	dry bulk density of litter
θ_l	volumetric liquid soil moisture content (m^3 m^{-3})
θ_r	residual volumetric soil moisture content (m^3 m^{-3})
θ_{sat}	saturated volumetric soil moisture content (m^3 m^{-3})
$\theta_{sat,L}$	saturated volumetric moisture content of litter (m^3 m^{-3})
τ	soil tortuosity (<1)

Subscripts

a	atmosphere
p	pond
w	water
l	liquid
v	vapour
s	surface
a	atmosphere
L	litter
P	pond
H	heat
w	water
sat	saturation

Superscript

i	isotope

In unsaturated soils, the depth of the peak in soil water isotope composition is associated with the depth of the evaporating front, i.e. the depth below which liquid transport and above which vapour transport is dominant (Barnes and Allison, 1983) The peak

in isotopic composition occurs because vapour transfer causes the remaining liquid water to be enriched due to equilibrium fractionation (preferential affinity of the lighter isotopologue for the vapour-phase) and kinetic fractionation (preferential diffusion of the lighter isotopologue). The vertical distribution of minor isotopologues is therefore sensitive to the vapour-phase component of the soil moisture flux. Despite this sensitivity, none of the hydrological schemes incorporated in current isotopically-enabled LSMs considers vapour-phase transfer of soil moisture: the most sophisticated of these (e.g. Riley et al., 2002; Yoshimura et al., 2006) treat vertical transport of soil moisture using Richards equation, which expresses the soil moisture flux between multiple soil layers as the sum of liquid suction and drainage terms, while simpler models (see examples in Henderson-Sellers et al., 2006) ignore the vertical distribution of soil moisture and isotopes altogether, by treating the entire soil moisture reservoir as a single bucket. The latter can lead to apparent fractionation factors that are not constant but change with time and soil water status (Braud et al., 2009a,b), which may in turn lead to erroneous conclusions of soil water isotope applications such as partitioning evapotranspiration.

In this work, we present Soil–Litter–Iso: a new one-dimensional model for coupled transport of heat, water and stable isotopes (HDO and $H_2{}^{18}O$) in soil and litter. Like SiSPAT-Isotope, it is based on the 1-dimensional coupled transport of heat and water in soil and therefore decomposes the total moisture flux into liquid and vapour components. In addition, the numerical implementation is faster than SiSPAT; ponding is included and there is an optional litter layer, which strongly inhibits soil evaporation. These attributes make the model suitable for incorporation into an LSM. We describe below the basic soil model (Section 2) and the incorporation of stable isotopes (Section 3). In Section 4 we present a series of test-cases which lend credibility to the model's numerical accuracy and robustness and in Section 5 we demonstrate the model's operation within an LSM by performing multi-year simulations for the Tumbarumba flux site, located in a tall Eucalyptus forest in south-eastern Australia.

2. Model description

2.1. The Soil–Litter model

The basic model (without isotopes) is presented in detail in Appendix A and described only briefly here. It is an extension of Ross' fast numerical solution (Ross, 2003) of Richards equation:

$$\frac{\partial \theta_l}{\partial t} = \frac{\partial}{\partial z}[-K(dh/dz) + K] - r_{ex} \tag{1}$$

which is a combination of Darcy's Law for vertical downward flow:

$$q_l = -K(dh/dz) + K \tag{2}$$

and the conservation equation for soil moisture:

$$\frac{\partial \theta_l}{\partial t} = \frac{\partial q_l}{\partial z} - r_{ex} \tag{3}$$

Features of Ross' model that have been retained include: discretisation in time and space; adaptive time stepping; calculation of liquid water fluxes in terms of the flux matric potential difference and an appropriately weighted drainage term (see Appendix A, Eq. (A.51)); treatment of saturated soil, surface runoff and ponding. Note that the weighting of the drainage term allows the model to be run using varying soil hydraulic properties with depth, without resorting to very small layer thicknesses. The major modification to Ross' model is that the vapour-phase water flux:

$$q_v = -D_v(dc_v/dz) \tag{4}$$

is added to the liquid flux and the conservation equation for energy is introduced:

$$\frac{c_{soil}\partial T}{\partial t} = \frac{\partial q_H}{\partial z} \tag{5}$$

with

$$q_H = -k_H\frac{dT}{dz} - \rho\lambda_E q_v \tag{6}$$

Since a component of the vapour-phase moisture flux is temperature-dependent, and a component of the heat flux depends on soil moisture potential, the equations for moisture and energy conservation are coupled. This leads to a set of $2n$ linear equations which are solved simultaneously for the changes over the time-step in relative soil moisture content and in temperature in each of n layers by inversion of a single sparse matrix. A further modification is that the surface boundary condition is specified at the beginning of each time step by solving the coupled energy and moisture conservation equations at the air/soil interface:

$$\begin{aligned}\frac{1}{r_{bw}}[h_{r,s}(c_{v,sat}(T_1) + s(T_1)(T_s - T_1)) - c_{v,a}] \\ = \frac{D_{v,1}}{dx_1/2}c_{v,sat}(T_1)(h_{r,1} - h_{r,s}) + \frac{D_{v,1}}{dx_1/2}s(T_1)h_{r,1}(T_1 - T_s) \\ + \left[\frac{(\phi_l(h_{r,1}) - \phi_l(h_{r,s}))}{dx_1/2} - K_1\right]\end{aligned} \tag{7}$$

$$\begin{aligned}R_{net} = \frac{\rho_a c_p}{r_{bh}}(T_s - T_a) + \frac{\rho\lambda_e}{r_{bw}}[h_{r,0}(c_{v,sat}(T_1) + s(T_1)(T_s - T_1)) - c_{v,a}] \\ - \frac{k_{H,1}}{dx_1/2}(T_1 - T_s)\end{aligned} \tag{8}$$

for surface temperature (T_s) and relative humidity ($h_{r,s}$). These variables are used in turn to calculate the heat and moisture fluxes at the surface. (In Eqs. (7) and (8), the subscript "1" refers to the top toil layer.)

An optional litter layer on top of the soil column reduces soil evaporation, because it does not permit upward movement of liquid water from the soil column to the litter layer or from within the litter layer to the surface. Transfer of water across the litter layer is restricted to vapour-phase transfer and downward drainage of liquid water from the litter to the soil column when the litter is saturated. The litter layer also insulates the soil column because it has a relatively low thermal conductivity. When a litter layer is present, we solve the coupled energy and moisture conservation equations (Eqs. (7) and (8)) both at the air/litter interface and at the litter/soil interface.

Ogée and Brunet (2002) and Gonzalez-Sosa et al. (1999, 2001) have demonstrated the importance of including litter on modelled soil evaporation in forest and agricultural ecosystems respectively. Our parameterisation of the litter layer is very similar to that of Ogée and Brunet (2002), who presented a forest floor model for heat and moisture including a litter layer. They showed that inclusion of litter in their model significantly improved prediction of soil temperature and moisture and components of the energy budget (H, λE, G) at the ground in a pine forest. The significant difference between the two parameterisations is that Ogée and Brunet set the evaporative flux from litter/soil interface to litter ($q_{evap,L}$) to zero, whereas we calculate it as a term in the energy and moisture conservation equations at the litter/soil interface.

Numerical efficiency has been achieved by developing Ross' fast non-iterative solution of the Richards' equation, which is 20–45 times faster than standard iterative methods (Ross, 2003) The computation time for Soil–Litter–Iso is approximately three times longer than for Ross' model, because we solve for two additional variables, namely change in soil temperature and change in isotopic concentration (see below). The optional litter layer increases computation time by about a factor of 3, particularly because of

the small heat capacity of the litter which necessitates the use of smaller time-steps.

2.2. Isotope transport in the Soil–Litter–Iso model

Treatment of stable isotopes in soil water is presented in detail in Appendix B and described briefly here. The solution for the change in minor isotopologue concentration, c_l^i, is performed separately, after the soil moisture and temperature have been updated in the main part of the code. Note here that all computations are performed with isotopologue concentrations in typical solute units of kg m^{-3} $H_2O_{(l)}$ and are converted to delta units (δ_i) for display purposes only. We use the classical definition of δ_i:

$$\delta_i = \frac{R_i - R_{ref}}{R_{ref}} \tag{9}$$

where

$$R_i = \frac{M_W}{M_i}\frac{c_l^i}{\rho} \tag{10}$$

and R_{ref} is a reference value corresponding to the molar isotopic ratio of Vienna Mean Standard Ocean Water (VSMOW, Gonfiantini, 1978).

The one-dimensional conservation equation for the minor isotopologue (HDO or $H_2{}^{18}O$) is:

$$\frac{\partial}{\partial t}\{c_l^i[\theta_l + \alpha^+ c_v(\theta_{sat} - \theta_l)]\} = -\frac{\partial}{\partial z}(q_l^i + q_v^i) - c_l^i r_{ex} \tag{11}$$

Where the liquid-phase flux of the minor isotopologue is the sum of advective and diffusive components:

$$q_l^i = c_l^i q_l - D_l^i \frac{dc_l^i}{dz} \tag{12}$$

and the vapour-phase flux of the minor isotopologue is a diffusive process which is expressed as a term which is proportional to q_v, plus contributions due to the vertical gradients in c_l^i and in α^+ (and therefore temperature):

$$\begin{aligned} q_v^i &= -D_v^i \frac{dc_v^i}{dz} = -D_v^i \frac{d(\alpha^+ c_l^i c_v)}{dz} \\ &= -D_v^i \alpha^+ c_l^i \frac{dc_v}{dz} - D_v^i c_v \left(\alpha^+ \frac{dc_l^i}{dz} + c_l^i \frac{d\alpha^+}{dz}\right) \\ &= \alpha_{k,diff}\alpha^+ c_l^i q_v - D_v^i c_v \alpha^+ \frac{dc_l^i}{dz} - D_v^i c_v c_l^i \frac{d\alpha^+}{dz} \end{aligned} \tag{13}$$

Substituting Eqs. (12) and (13) into Eq. (11) and rewriting it in discrete form leads to a set of n linear equations which can be solved simultaneously for Δc_l^i in each layer by a single tridiagonal matrix inversion.

The surface boundary flux of the minor isotopologue is evaluated as:

$$q_0^i = c_{prec}^i q_{prec} - (c_{evap,out}^i q_{evap,out} - c_{evap,in}^i q_{evap,in}) \tag{14}$$

with

$$q_{evap,out} = c_{v,s}/r_{bw} \tag{15}$$

$$q_{evap,in} = c_{v,a}/r_{bw} \tag{16}$$

$$c_{evap,out}^i = \alpha_k \alpha^+(T_s) c_{l,s}^i \tag{17}$$

$$c_{evap,in}^i = \alpha_k \rho R_a M_i / M_w \tag{18}$$

In Eqs. (14)–(18), "in" and "out" refer to the gross (one-way) fluxes from the atmosphere to the surface and from the surface to the atmosphere respectively.

The surface concentration of the minor isotopologue ($c_{l,s}^i$), which is required to evaluate $c_{evap,out}^i$, is obtained from the conservation equation for the minor isotopologue at the air/soil interface:

$$\begin{aligned} \frac{\alpha_k}{r_{bw}}(c_{v,s}c_{l,s}^i\alpha^+(T_s) - c_{v,a}^i) = \alpha_{k,diff}\frac{D_{v,1}}{\Delta x_1/2}(c_{v,1}\alpha^+(T_1)c_{l,1}^i - c_{v,s}c_{l,s}^i\alpha^+(T_s)) \\ - q_{l,0}(w_s c_{l,s}^i + w_1 c_{l,1}^i) + \frac{D_{l,1}^i}{\Delta x_1/2}(c_{l,1}^i - c_{l,s}^i) \end{aligned} \tag{19}$$

Explicit resolution of the isotopic concentration at the air/soil interface allows a much thicker top soil layer than could be used if equal concentrations at the surface and within the top soil layer were assumed.

3. Test cases vertical isotopic concentration profiles

3.1. Plausibility test-cases

Mathieu and Bariac (1996) designed six test-cases for the purpose of checking that the model produces plausible results as sources of isotopic fractionation in the model are switched on sequentially. Braud et al. (2005a) also used these test-cases as qualitative tests of SiSPAT-Isotope. Here we repeat the test-cases for Soil–Iso–Litter. Following Braud et al. (2005a), we consider a 1 m soil column with properties of Yolo Light clay ($\theta_{sat} = 0.35$; $\theta_r = 0.01$; $\lambda = 0.22$; $\eta = 9.14$; $K_{sat} = 1.23 \times 10^{-7}$; $h_e = -0.193$) initially saturated with uniform isotopic concentration δ_{ali} and temperature 303 K. It is exposed to an atmosphere with $T_a = 303$ K, $h_{r,a} = 0.2$ and water vapour isotopic concentration δ_a^v for 250 days. Net radiation absorbed by the soil was set to zero, leading to approximately isothermal conditions. We used a zero-flux bottom boundary condition for soil moisture and isotope fluxes, which contrasts to the normal free drainage fluxes. Fluxes at the soil surface were determined as normal, by solving the coupled energy and moisture balances at the air/soil interface. For these tests, the soil was divided into 20 layers, with a top layer thickness of 9 mm. The conditions for each test are listed in Table 1 and the corresponding vertical concentration profiles of the minor isotopologues at the end of the 250 day period are shown in Fig. 1. Formulations of α^+ and α_k are given in Appendix B.7. Note that, for consistency with Braud et al. (2005a) and Mathieu and Bariac (1996), the values of D_v^i (which are also used to evaluate α_k) in Test 6, and in comparisons with steady-state analytical solutions (Sections 3.2 and 3.3), are those measured by Merlivat (1978). Elsewhere in this work, we use the updated values of D_v^i measured by Cappa et al. (2003).

In Test (1), the isotopic ratio of atmospheric water vapour is set equal to that of the initial soil water; equilibrium and kinetic fractionation factors are set to one and liquid diffusion of the minor isotopologue is set to zero. As expected, the result is a uniform concentration profile. The small standard deviation of 2×10^{-15}‰ is indicative of the model's numerical robustness, and contrasts with

Table 1
Plausibility tests.

Test	α^+	D_v^i	D_l^i	α_k	δ_a^v
(1)	1	D_v	0	1	δ_{ali}
(2)	1	D_v	0	1	δ_a^v
(3)	α^+	D_v	0	1	δ_{ali}
(4)	α^+	D_v	0	1	δ_a^v
(5)	α^+	D_v	D_l^i	1	δ_a^v
(6)	α^+	D_v^i	D_l^i	α_k	δ_a^v

$\delta_{ali}(D) = -65$‰; $\delta_{ali}(^{18}O) = -8$‰; $\delta_a^v(D) = -112$‰; $\delta_a^v(^{18}O) = -15$‰.

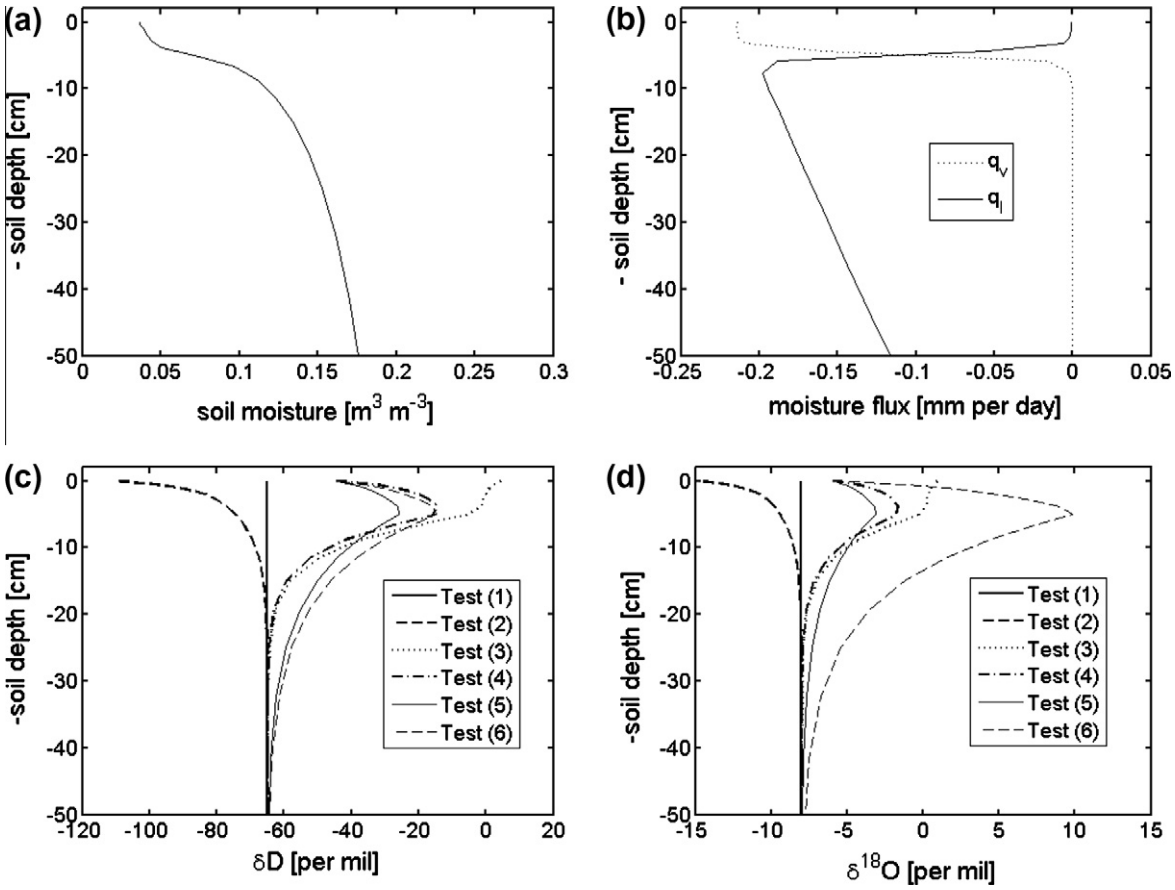

Fig. 1. Plausibility tests 1–6: simulations at end of 250-day period. Vertical profiles of (a) soil moisture; (b) liquid and vapour components of the moisture flux; (c) HDO concentration; (d) $H_2{}^{18}O$ concentration.

the much larger deviation (0.15‰) obtained using SiSPAT-Isotope with a much smaller (1×10^{-3} mm) top layer.

Test (2) is the same as Test (1), except that the isotopic ratio in the atmospheric water vapour is given a realistic value which is significantly lower than that of the initial soil water. The result is that the isotopic concentration in the surface soil moisture approaches that in the atmospheric water vapour and increases smoothly with depth to its initial value due to vapour diffusion.

Test (3) is the same as Test (1), except that equilibrium isotopic fractionation is turned on both within the soil column and at the surface. The latter determines the isotopic enrichment in the soil surface water. The rapid increase in isotopic enrichment with height in the region below 5 cm is attributable to the large vapour flux divergence, combined with equilibrium isotopic fractionation in this region. Above 5 cm, the vapour flux is approximately constant, so that equilibrium isotopic fractionation within the soil has a smaller effect on the profile and there is a gradual transition to the surface value.

Test (4) is the same as Test (3), except that the isotopic ratio in the atmospheric water vapour is reset to a realistic value, which shifts the isotopic enrichment at the surface to a lower value. This surface effect, combined with the increasing enrichment with height due to equilibrium fractionation in the region of large vapour flux divergence leads to the observed maximum in isotopic enrichment.

Test (5) is the same as Test (4), except that liquid diffusion is turned on, which leads to a smearing of the isotopic concentration profile and hence a broader peak with a smaller height.

Test (6) is the same as Test (5) except that kinetic fractionation at the surface is switched on and the isotopic water vapour diffusivity is set to its true value. The former has the effect of shifting the enrichment at the surface to a slightly higher value. The major difference between the shapes of the profiles in Tests (5) and (6), (namely a higher peak) is attributable to the isotopic vapour diffusivity, which is smaller for the heavier isotopologue. Since vapour "advection" (see first term in Eq. (B.4)) within the soil column is actually a diffusive process, the higher diffusivity of the lighter isotopic species leads to its preferential removal in the region of vapour flux divergence, which increases the isotopic enrichment in the remaining liquid soil moisture, leading to a bigger peak in the concentration profile.

The simulations above highlight the importance of including vapour-phase movement within the soil column. Without this process, neither equilibrium fractionation nor diffusional fractionation of the isotopologues within the soil column could be simulated and the maximum in the isotopic concentration profiles, which coincides with the sharp decrease in soil moisture (Fig. 1a) and the transition from liquid to vapour-dominated flux (Fig. 1b), could not be reproduced.

3.2. Comparison with steady-state analytical solution: isothermal saturated case

Barnes and Allison (1983) derived an analytical solution for the steady-state isotopic concentration profile in a saturated soil column. Steady-state is achieved by constantly re-alimenting the soil column from the bottom with water of constant isotopic concentration $c^i_{l,ali}$ at a rate equal to the evaporation rate. The vertical isotopic ratio profile is then:

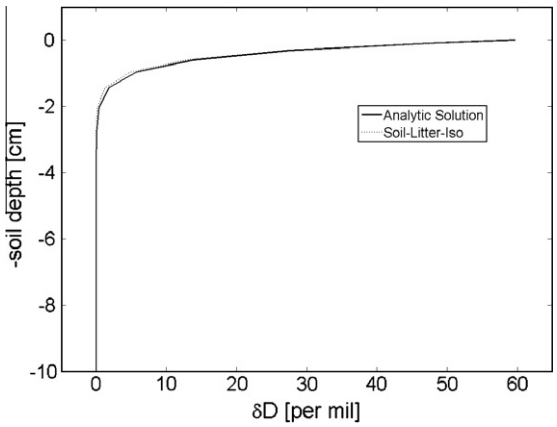

Fig. 2. HDO concentration profile for saturated soil column at equilibrium: simulations from Soil–Litter–Iso and from the analytic solution of Barnes and Allison (1983).

$$c_l^i(z,t) = c_{l,ali}^i + (c_{l,s}^i - c_{l,ali}^i)\exp\left(-\frac{\rho q_{evap}}{D_l^i} z\right) \tag{20}$$

We simulated the steady-state isothermal saturated profile with Soil–Iso–Litter using the same soil column and conditions as for Test (6) above, except that the bottom boundary condition was changed so that $q_n = -q_{evap}$ and $c_{l,n}^i = c_{l,ali}^i$. Results for HDO are compared in Fig. 2. The excellent agreement (to within 0.5‰) illustrates good numerical accuracy under saturated conditions.

3.3. Comparison with steady-state analytical solution: non-isothermal unsaturated case

Barnes and Allison (1984) derived a differential equation for the isotopic ratio profile at steady-state under non-isothermal unsaturated conditions:

$$h_r z_v R_i\left[\left(1-\frac{\alpha^+}{\alpha_{k,diff}}\right)\frac{d}{dz}\{\ln(h_r \rho c_{v,sat})\} - \frac{\alpha^+}{\alpha_{k,diff}}\frac{d}{dz}\{\ln(\alpha^* R_i)\}\right] = R_i - R_{ali} + \frac{z_l}{D_l^i}\frac{dR_i}{dz} \tag{21}$$

where

$$R_i = \frac{c_l^i}{\rho}\frac{M_w}{M_i} \tag{22}$$

$$z_v = \frac{D_v^i c_{v,sat}}{q_{evap}} \tag{23}$$

$$z_l = \frac{D_l^i}{q_{evap}} \tag{24}$$

We tested the model against Eq. (21) as follows. Conditions for Soil–Litter–Iso were the same as for the steady-state saturated case above, except that the initial soil moisture content was set to 0.7 of its saturated value; net radiation absorbed by the soil was set to 200 W m^{-2} and the heat flux at the lower soil boundary was set equal to the heat flux into the top of the soil column. Results are shown in Fig. 3. The steady-state soil moisture profile exhibits

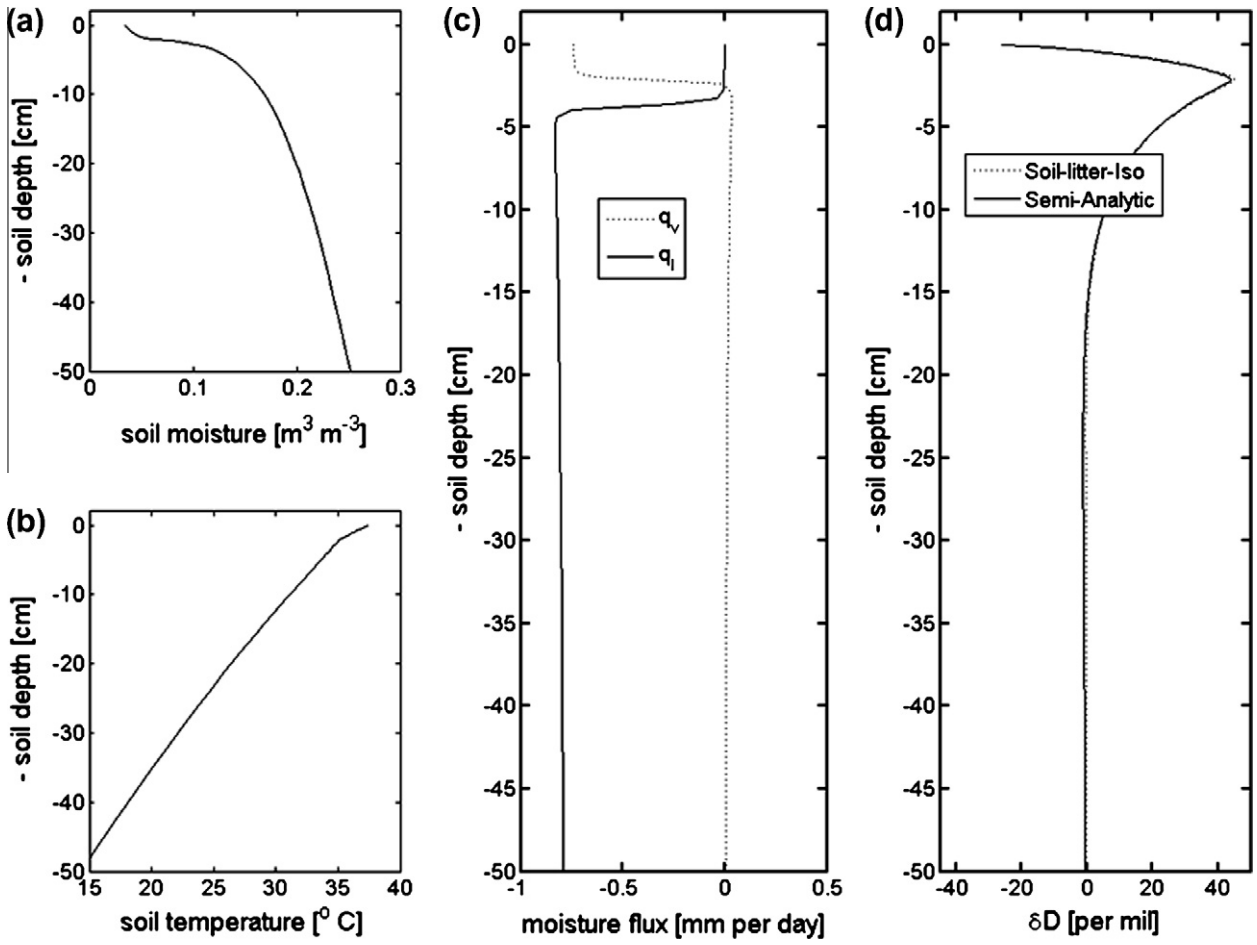

Fig. 3. Vertical profiles for non-isothermal unsaturated soil column at equilibrium: (a) volumetric soil moisture content; (b) soil temperature; (c) liquid and vapour components of moisture flux; (d) HDO concentration profiles from Soil–Litter–Iso and from semi-analytic solution of Barnes and Allison (1984).

an inflexion point at a depth of about 2 cm, corresponding to the evaporating front. It is also the point at which the upward flux of soil moisture switches from being predominantly liquid-phase to predominantly vapour-phase, and there is an accompanying maximum in the isotopic concentration profile. The temperature profile, which increases with depth, produces a positive contribution to q_{vap} (note the slightly positive values of q_{vap} at depths of around 5 cm), which influences the isotopic concentration profile via Eq. (B.4). The Semi-Analytic solution was obtained by solving Eq. (21) numerically, using cubic spline interpolating functions for each of the depth-dependent input variables h_r, α^+, $c_{v,sat}$, D_v^i, which were created from Soil–Litter–Iso output. The result agrees very well (to within 0.5‰) with Soil–Litter–Iso, indicating that the model is numerically accurate for unsaturated, non-isothermal conditions.

3.4. Robustness to soil layer thickness

A key advance of Soil–Litter–Iso over SiSPAT-Isotope and its predecessors, is that it is sufficiently robust to be run with relatively coarse layering (top soil layer 2 cm) and time-step (1 h), which leads to computational efficiency and hence versatility. Fig. 4 illustrates the model's robustness to soil layer thickness during drying. We choose a drying period because the development of a pronounced peak in the isotopic profile provides a stringent test. (In the case of soil wetting, the minor isotopic species behaves as a noninteracting solute, for which Ross (2003) has already demonstrated robust model performance using thick soil layers.) In Fig. 4a, we compare two steady-state isotopic concentration profiles, both generated using the same conditions as for the unsaturated non-isothermal testcase above. The simulation performed with only 10 soil layers and a top soil layer of 0.02 m compares very favourably (to within 0.5‰) with that obtained with 70 layers and a top soil layer of 10^{-4} m. In Fig. 4b, we repeat the simulations using a dual-horizon soil column. The top 23 cm have the properties of a sandy soil, and the remainder of the 180 cm soil column is a clayey soil, with clayey and sandy soil hydraulic properties taken from Ross (2003). Here we see that results of simulations with 20 layers (top soil layer 0.8 cm) agree well (to with 3‰) of results of simulations with 70 layers. However the 10-layer-scheme (results not shown) only agreed with the 70-layer-scheme to within 10‰. Thus, while the model's accuracy is extremely good for the coarse 10-layer-scheme when there is a single soil type, higher vertical resolution is required when there is more than one soil type. Nevertheless, the vertical resolution of the 20-layer-scheme, shown to be satisfactory for the dual-horizon soil, is still much coarser than the used in SiSPAT-Isotope [soil layer thicknesses of 10^{-6}–10^{-4} m near the surface (Braud et al., 2005a)]. The ability to use thicker surface layers in Soil–Litter–Iso is achieved by solving for surface temperature, humidity and isotopic concentration at the soil/air interface, which is necessary because the isotopic concentrations tend to vary steeply with soil depth near the surface, and therefore the concentrations at the surface and within the top soil layer need to be distinguished.

4. Dynamic simulations with and without litter at the Tumbarumba flux site

Finally we show results of multi-year simulations for the Tumbarumba flux site (Leuning et al., 2005), situated in a tall Eucalypt forest in south-eastern Australia. Here, total evapotranspiration

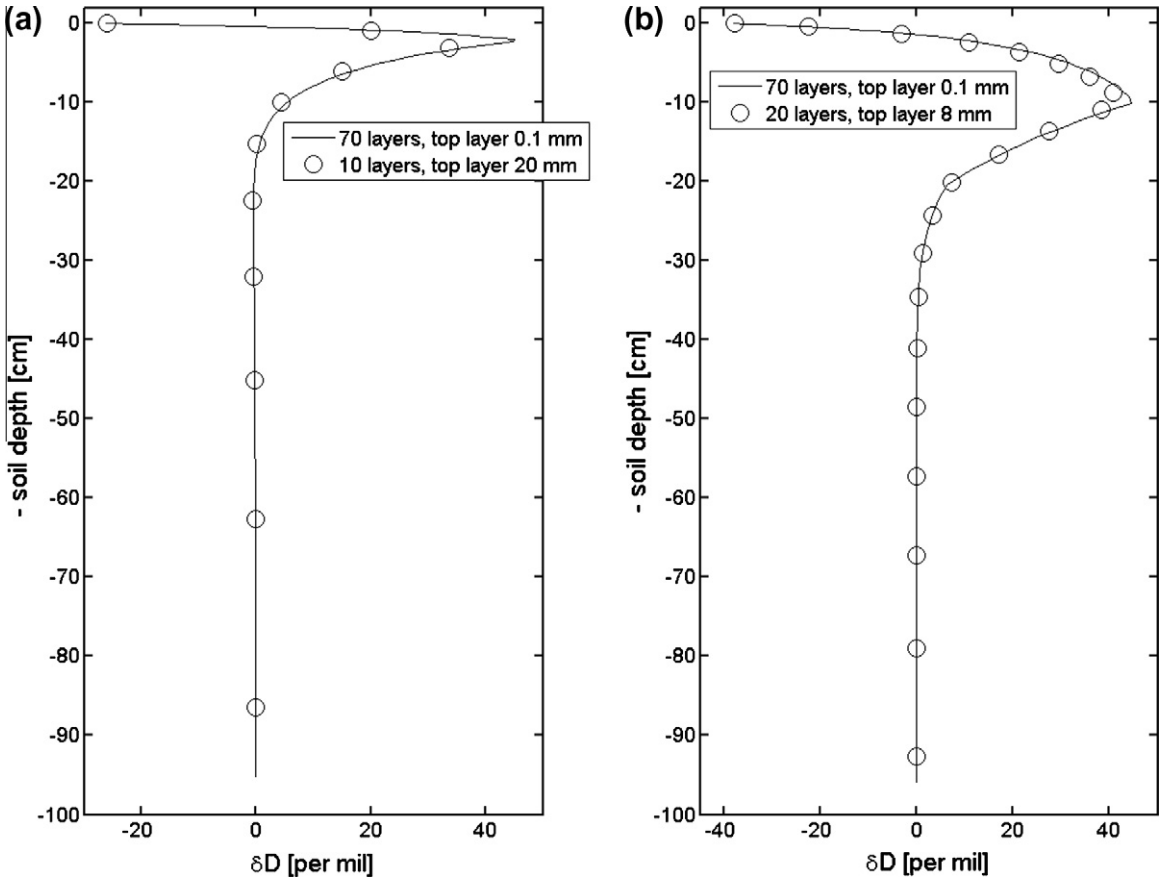

Fig. 4. Steady-state unsaturated non-isothermal HDO concentration profile simulated using different layering schemes. (a) soil properties for Yolo light clay; (b) dual-horizon soil column with top 23 cm sandy soil and clayey soil underneath.

above the canopy is measured continuously by eddy covariance and volumetric soil moisture (0–120 cm at depth resolution 15 cm) is measured continuously by time domain reflectometry. For these simulations, Soil–Litter–Iso was incorporated into an LSM called CABLE (Kowalczyk et al., 2006), which was forced using hourly meteorological data ($h_{r,a}$; T_a; windspeed; incoming shortwave and longwave radiation, precipitation). Measurements were unavailable for the $H_2{}^{18}O$ concentrations of atmospheric water vapour and precipitation and respective constant values of $-15‰$ and $-8‰$ were assumed. (Note here that these values are arbitrary and the resulting simulations of $H_2{}^{18}O$ in the soil evaporate are not intended to reflect reality, but to illustrate the sensitivity of the model predictions to the inclusion of litter.) The bottom boundary conditions were free drainage and zero heat flux. Vegetation parameters were set to those values obtained in an earlier study at this site (Haverd et al., 2009) by parameter estimation using multiple constraints. A 2-horizon soil column of depth 10 m was used, with parameters based on the Atlas of Australian Soils (McKenzie and Hook, 1992). Parameter values for the upper horizon (top 30 cm) were: ($\theta_{sat} = 0.47$; $\theta_w = 0.14$, $\theta_r = 0$, $\lambda = 0.29$; $\eta = 9.9$; $K_{sat} = 5.3 \times 10^{-5}$; $h_e = -0.364$) and for the remainder of the soil column: ($\theta_{sat} = 0.44$; $\theta_w = 0.15$, $\theta_r = 0$, $\lambda = 0.15$; $\eta = 16.3$; $K_{sat} = 2.03 \times 10^{-5}$; $h_e = -0.266$). Simulations were performed with and without a litter layer. Litter parameter values: $\theta_{sat,L} = 0.09$ and $\rho_{b,L} = 63.5$ kg m^{-3} were set in accordance with the Eucalpytus litter properties described by Matthews (2005). The litter layer depth was set to 3 cm, consistent with the above bulk density and measured dry litter mass (Heather Keith, pers. comm.).

Root-water uptake was modelled as:

$$r_{ex}(\theta, z) = \alpha(\theta) g(z) q_{trans} \tag{25}$$

where $\alpha(\theta)$ is the root efficiency function of Lai and Katul (2000), $g(z)$ is the vertical root density distribution of Li et al. (1999). (See Appendix C for full description.) Hourly values of the actual transpiration rate, q_{trans}, were derived from CABLE's sunlit/shaded two-leaf model (Wang and Leuning, 1998) which couples stomatal conductance, photosynthesis and energy partitioning in response to radiation absorption, temperature, water vapour pressure deficit at the leaf surfaces and soil moisture. Stomatal conductance is assumed to vary linearly with a function of soil moisture, $f(\theta)$, which, for consistency with root extraction, was set here to:

$$f(\theta) = \int_0^L \alpha(\theta) g(z) dz \tag{26}$$

where L is the depth of the soil column.

CABLE was run at an hourly time-step, and Soil–Litter–Iso was called at each time-step from within CABLE. Transpiration and hence root extraction rates were assumed to remain constant for the duration of each hourly time-step.

Model results, along with eddy flux measurements of total evapotranspiration (ET) and time domain reflectometry measurements of volumetric soil moisture content in the top 15 cm, are shown as 30-day running means in Fig. 5. We plot volumetric soil moisture content as an anomaly (i.e mean value over 2001–2009 subtracted) because of the high uncertainty in the absolute value of the observations. The model with litter better reproduces the observed seasonal dynamics of total evapotranspiration (ET) (Fig. 5a) than the model without litter. Neither model has been calibrated and it is therefore not possible to argue conclusively that the model with litter is superior. However it is likely that the inclusion of litter improves model performance at this site because the improved timing of the modelled ET peaks when litter is included is interpretable in terms of process description as follows. The model without litter over-predicts ET in spring each year because of the significantly larger contribution from soil evaporation

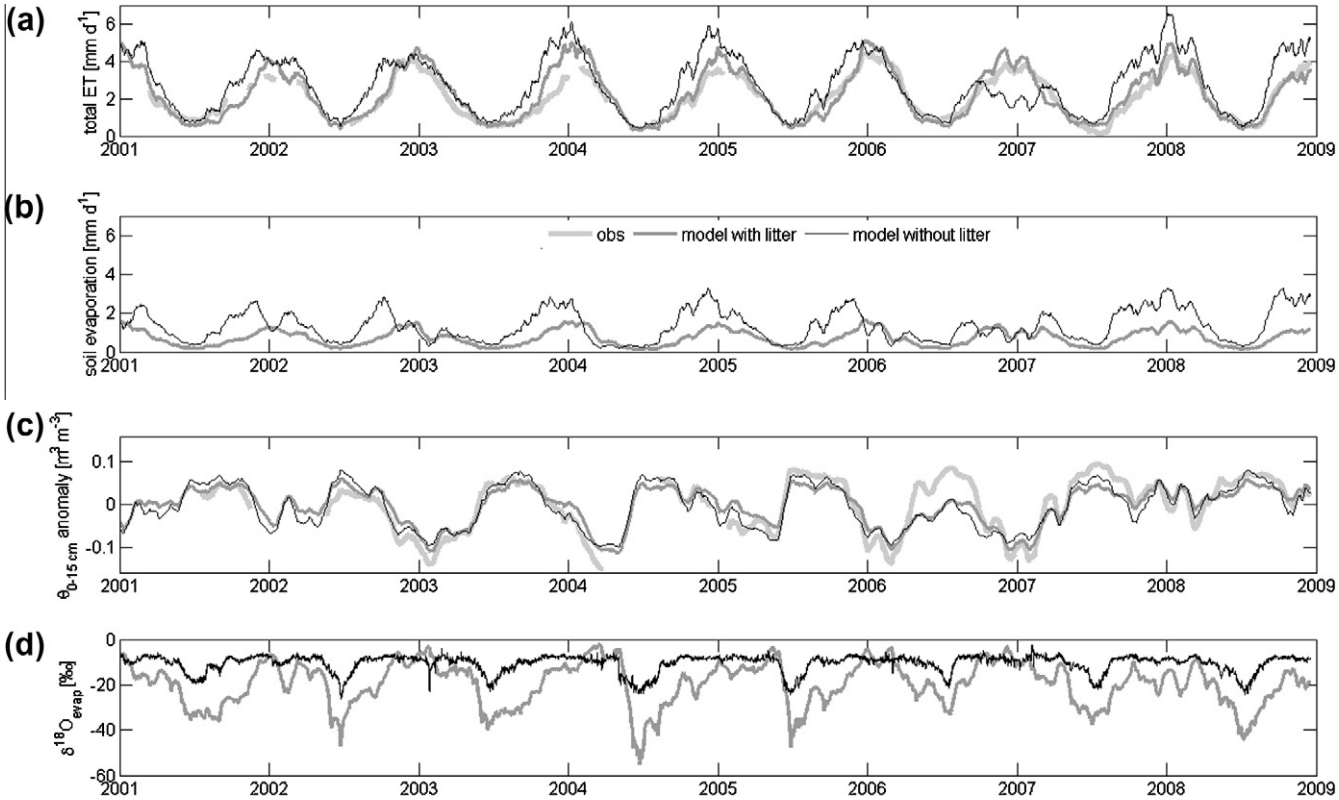

Fig. 5. 30-day running mean times series for the Tumbarumba flux site. (a) Total evapotranspiration, (b) soil evaporation and (c) volumetric soil moisture (0–15 cm) anomaly (2001–2009 mean subtracted) (d) $\delta^{18}O$ in H_2O for soil evaporate. Thick light grey lines are observations, medium grey lines are predictions of the model with the litter layer, thin black lines are the predictions of the model without litter.

(Fig. 5b) and is unable to capture the observed peak in ET in the dry summer of 2006–2007 because higher soil evaporation rates leave less soil moisture available for transpiration. (Note this is not evident in Fig. 5c because here soil moisture is plotted as anomaly.) Both models generally capture the soil moisture dynamics well (Fig. 5c), except in the winter of 2006 when both models significantly underpredict the anomaly and mean annual precipitation was 40% of the 1990–2009 average. This points to model deficiency in the root water uptake, given the good predictions of total ET during this period. Model predictions for the 0–120 cm column are in much better agreement with observations (results not shown), indicating that the model is over-extracting water from the top 15 cm. In Fig. 5d we plot the $H_2{}^{18}O$ concentration of the soil evaporate (in δ-units). The corresponding values for the transpirate ($-6.4 \pm 0.5‰$ for the model with litter and $-7.3 \pm 0.17‰$ for the model without litter) (not shown) are consistently close to those of the bulk soil ($-8‰$). The soil evaporate slowly approaches this value as the soil dries out and ET reaches its seasonal peak. It is then challenging to discriminate between soil evaporation and plant transpiration with isotopes. However the approach time for the model with litter ($\sim$3 months) is about twice as long as for the one without and there are more frequent periods when the isotopic signatures of the ET components are distinct.

5. Conclusions

Soil–Litter–Iso represents an advance upon currently available models for the coupled transport of soil moisture, heat and isotopes, insofar as it combines advanced process description, numerical accuracy and numerical efficiency. The process description includes vapour-phase transfer of soil moisture and inhibition of soil evaporation by litter, which have not previously been accounted for in isotopically-enabled LSMs. The plausibility test-cases (Fig. 1) show that the isotopic soil profiles are sensitive to isotopic fractionation during vapour-phase diffusion and equilibration between liquid and vapour phases within the soil column. The inclusion of these fractionation effects is conditional upon the inclusion of vapour-phase transfer within the soil column. Numerical accuracy has been tested by comparing model output with steady-state analytical solutions for both isothermal flow under saturated conditions and non-isothermal flow under unsaturated conditions. The excellent agreement was as good or better than that obtained by earlier models. Numerical efficiency has been achieved by using Ross' fast non-iterative solution of the Richards' equation, which is 20–45 times faster than standard iterative methods (Ross, 2003). The computation time for Soil–Litter–Iso is approximately three times longer than for Ross' model, because we solve for two additional variables, namely change in soil temperature and change in isotopic concentration. Robustness to surface soil layer thickness, as demonstrated in Fig. 4, is achieved by solving for surface temperature, humidity and isotopic concentration at the soil/air interface. Simulations for the Tumbarumba flux site (Fig. 5) demonstrated the model's operation within an LSM. They indicated that the components of the water balance are highly sensitive to the presence of litter, and that the model with litter is better able to reproduce observed total evapotranspiration at this site. Simulations of $\delta^{18}O$ of the soil evaporation and plant transpiration fluxes showed isotopic signatures of the transpirate which were consistently close to those of the bulk soil water, while the $\delta^{18}O$ of the soil evaporate tended to slowly approach this value over a drying period (1–3 months). The simulations without litter (higher soil evaporation rates and drier soil) showed much more extended periods of approximately equal signatures for soil evaporate and plant transpirate than the simulations with litter. Such simulations are useful for assessing when the isotopic signatures are sufficiently distinct to partition ET into its component fluxes. However, the model is a one-dimensional representation of reality and in addition has the same restrictions as any hydrologic model. Namely, most parameters, e.g. in the Brooks and Corey relations, are effective parameters over the soils heterogeneity. The same is true for new parameters introduced in Soil–Litter–Iso, e.g. the litter parameters saturated volumetric moisture content ($\theta_{sat,L}$) and dry bulk density ($\rho_{b,L}$). Further uncertainty arises via uncertainty in process description. Most prominent is root water uptake (c.f. Feddes et al., 2001). Soil–Litter–Iso adapts but is not limited to the root water uptake model of Lai and Katul (2000). Any other root uptake model can be implemented. In the isotopic part of the model, the kinetic fractionation at the soil/air interface is another example of uncertain process knowledge (Braud et al., 2005b). Again, the adopted formulation is only a suggestion that can be changed easily in the model.

Acknowledgements

We gratefully acknowledge Peter Ross for supplying the code for his soil model, which was used as the starting point to develop Soil–Litter–Iso. Cathy Trudinger, Mike Raupach and Luigi Renzullo kindly reviewed the manuscript and provided helpful suggestions. This work was supported in part by a grant from the Australian Climate Change Science Program.

Appendix A. Soil–Litter model description

The time evolutions of soil moisture θ and temperature T, and hence moisture and energy exchange between the soil and the atmosphere, are estimated by solving the following one-dimensional conservation equations for soil moisture and energy:

$$\frac{\partial\theta}{\partial t} = \frac{\partial q_w}{\partial z} - r_{ex} \tag{A.1}$$

and

$$\frac{c_{soil}\partial T}{\partial t} = \frac{\partial q_H}{\partial z}. \tag{A.2}$$

Solution of these equations requires formulations of the moisture flux q_w and heat flux q_H, boundary conditions and a numerical solution method, which are described below.

A.1. Moisture and heat fluxes within soil column

The vertical flux (positive downwards) of liquid water q_l is the sum of transport due to a gradient in pressure head h and transport by gravitational drainage (hydraulic conductivity K):

$$q_l = -K(dh/dz) + K = d\phi_l/dz + K \tag{A.3}$$

The temperature dependence of the liquid water flux q_l is negligible and will not be considered here. In Eq. (A.3), the matric flux potential φ_l is calculated from the Kirchhoff transform when the soil is unsaturated:

$$\phi_l = \int_{-\infty}^{h} K(\bar{h})d\bar{h} = \int_{-\infty}^{h} K_{sat}\left(\frac{\bar{h}}{h_e}\right)^{-\lambda\eta} d\bar{h} = \frac{K_{sat}h_e}{1-\lambda\eta}\left(\frac{h}{h_e}\right)^{1-\lambda\eta} \tag{A.4}$$

It is used because it linearises the pressure head term in Eq. (A.3), allowing discretised flux calculations to be performed accurately over much larger distances than if h is used. For saturated soil,

$$\phi_l = \frac{K_{sat} h_e}{1 - \lambda\eta} \tag{A.5}$$

We use the Brooks and Corey relations (Brooks and Corey, 1964) to define the soil moisture retention

$$S = \frac{\theta - \theta_r}{\theta_{sat} - \theta_r} = \left(\frac{h}{h_e}\right)^{-\lambda}, \quad h < h_e = 1, \quad h \geqslant h_e \tag{A.6}$$

and hydraulic conductivity curves:

$$\frac{K}{K_{sat}} = S^{\eta}, \quad h < h_e = 1, \quad h \geqslant h_e \tag{A.7}$$

with the shape parameters either independently specified or related by (Campbell, 1974):

$$\eta = 2/\lambda + 3 \tag{A.8}$$

The vertical flux of water vapour, q_v is

$$q_v = -D_v(dc_v/dz) \tag{A.9}$$

with D_v the diffusivity of water vapour in the bulk soil

$$D_v = D_{v,a}\tau(\theta_{sat} - \theta_l) \tag{A.10}$$

and $D_{v,a}$ the diffusivity of water vapour in air which depends on atmospheric pressure and temperature (De Vries, 1975):

$$D_{v,a} = D_{v,0}\frac{10^5}{p_{atm}}\left(\frac{T + 273.15}{273.15}\right)^{1.88} \tag{A.11}$$

It is convenient to separate the water vapour flux into components driven by gradients in relative humidity, h_r, (and hence pressure head, h) and saturated vapour pressure, $c_{v,sat}$, (and hence temperature):

$$q_v = q_{v,h} + q_{v,T} = -\left(D_v c_{v,sat}\frac{dh_r}{dz} + D_v h_r \frac{dc_{v,sat}}{dz}\right) \tag{A.12}$$

The dependence of saturated vapour pressure $c_{v,sat}$ on T is calculated from Teten's formula (Ham, 2005):

$$c_{v,sat} = 610.78\exp(17.27T/(T + 237.2))M_W R/\rho/(T + 273.16) \tag{A.13}$$

And we assume equilibrium between liquid and vapour water, such that the dependence of h_r on h is given by (Philip, 1957):

$$h_r = \exp(M_w hg/RT) \tag{A.14}$$

We rewrite $q_{v,h}$ in terms of $\frac{dh}{dz}$:

$$\begin{aligned} q_{v,h} &= -D_v c_{v,sat}\frac{dh_r}{dh}\frac{dh}{dz} \\ &= -D_{v,0}\left(\frac{T + 273.16}{273.16}\right)^{1.88}(\theta_{sat} - \theta)\tau c_{v,sat} c h_r \frac{dh}{dz} \\ &= -D_{v,0}\left(\frac{T + 273.16}{273.16}\right)^{1.88}\tau c_{v,sat}\frac{d\phi_v}{dz} \end{aligned} \tag{A.15}$$

where $D_{v,0}$ is the diffusivity of water vapour in air at 0 K ($D_{v,0} = 2.12 \times 10^{-5}\ \mathrm{m^2\ s^{-1}}$),

$$c = \frac{M_W g}{RT} \tag{A.16}$$

$$\begin{aligned} \phi_v &= \int_{-\infty}^{h}(\theta_{sat} - \theta(h))dh_r = \int_{-\infty}^{h}(\theta_{sat} - \theta(h))\frac{dh_r}{dh}dh \\ &= \int_{-\infty}^{h}(\theta_{sat} - \theta(h))ce^{ch}dh \end{aligned} \tag{A.17}$$

Substitution of Eq. (A.6) into Eq. (A.17) yields

$$\begin{aligned} \phi_v &= (\theta_{sat} - \theta_r)\left(e^{ch} - \int_{-\infty}^{h}\left(\frac{h}{h_e}\right)^{-\lambda} ce^{ch}dh\right) \\ &= (\theta_{sat} - \theta_r)(e^{ch} - ch_e\gamma(1 - \lambda, -ch)) \end{aligned} \tag{A.18}$$

with γ the incomplete gamma function:

$$\gamma(a, z) = \int_z^{\infty} t^{a-1}e^{-t}dt \tag{A.19}$$

The total water flux, is then:

$$\begin{aligned} q_w &= -\frac{d\phi_l}{dz} + K - D_{v,0}\left(\frac{T + 273.16}{273.16}\right)^{1.88}\tau c_{v,sat} c\frac{d\phi_v}{dz} - \eta_E D_v h_r s\frac{dT}{dz} \\ &= -\frac{d\phi_l}{dz} + K - k_{v,h}\frac{d\phi_v}{dz} - k_{v,T}\frac{dT}{dz} \end{aligned} \tag{A.20}$$

with

$$k_{v,h} = D_{v,0}\left(\frac{T + 273.16}{273.16}\right)^{1.88}\tau c_{v,sat} \tag{A.21}$$

and

$$k_{v,T} = \eta_E D_v h_r s \tag{A.22}$$

A dimensionless enhancement factor, η_E, is introduced because the observed transport of water vapour in a temperature gradient generally exceeds that predicted by Eq. (A.12). The enhancement factor has the form (Campbell, 1985):

$$\eta_E = A + B\theta - (A - D)\exp(-(C\theta)^E) \tag{A.23}$$

with $A = 9.5,\ B = 6,\ C = 1 + 2.6f_c^{-1/2},\ D = 1,\ E = 4$ and f_c the fraction of clay in the soil.

The vertical heat flux is the sum of sensible and latent heat fluxes:

$$q_H = -k_H\frac{dT}{dz} - \rho\lambda_E q_v = -(k_H + \rho\lambda_E k_{v,T})\frac{dT}{dz} - \rho\lambda_E q_{v,h} \tag{A.24}$$

Here k_H is the moisture-dependent thermal conductivity of the soil, which is modelled according to Campbell (1985):

$$k_H = A + B\theta - (A - D)\exp[-(C\theta)^E] \tag{A.25}$$

where

$$A = 0.65 - 0.78(\rho_b/1000) + 0.60(\rho_b/1000)^2 \tag{A.26}$$

$$B = 1.06(\rho_b/1000)\theta \tag{A.27}$$

$$C = 1 + 2.6f_c^{-1/2} \tag{A.28}$$

$$D = 0.03 + 0.1(\rho_b/1000)^2 \tag{A.29}$$

and $E = 4$.

A.2. Discretisation

In order to solve Eqs. (A.1) and (A.2) numerically, we need to discretise them in space and time. The soil is divided into n horizontal layers of thicknesses dx_j, $j = 1, 2, \ldots, n$. The moisture balance equation for layer j is:

$$\frac{dx_j(\theta_{r,j} + (\theta_{sat,j} - \theta_{r,j})\Delta S_j)}{\Delta t} = q^{\sigma}_{w,j-1} - q^{\sigma}_{w,j} - r_{ex,j} \tag{A.30}$$

where $r_{ex,j}$ is the rate of water uptake by roots in the j^{th} layer and $q^{\sigma}_{w,j}$ is the flux from layer j to layer $j + 1$ evaluated at a fraction σ through the time step by linearisation in terms of S_j and S_{j+1}, T_j and T_{j+1}.

$$q^{\sigma}_{w,j} = q^{0}_{w,j} + \sigma\left(\frac{\partial q_{w,j}}{\partial S_j}\bigg|^0\Delta S_j + \frac{\partial q_{w,j}}{\partial S_{j+1}}\bigg|^0\Delta S_{j+1} + \frac{\partial q_{w,j}}{\partial T_j}\bigg|^0\Delta T_j + \frac{\partial q_{w,j}}{\partial T_{j+1}}\bigg|^0\Delta T_{j+1}\right), \quad j = 1, \ldots, n-1 \tag{A.31}$$

Substituting Eq. (A.31) into (A.30) leads to a set of n linear equations:

$$a_j\Delta S_{j-1} + b_j\Delta T_{j-1} + c_j\Delta S_j + d_j\Delta T_j + e_j\Delta S_{j+1} + f_j\Delta T_{j+1} = g_j, \quad j = 1,\ldots,n \tag{A.32}$$

with

$$a_j = \left.\frac{\partial q_{w,j-1}}{\partial S_{j-1}}\right|^0 \tag{A.33}$$

$$b_j = \left.\frac{\partial q_{w,j-1}}{\partial T_{j-1}}\right|^0 \tag{A.34}$$

$$c_j = \left.\frac{\partial q_{w,j-1}}{\partial S_j}\right|^0 - \left.\frac{\partial q_{w,j}}{\partial S_j}\right|^0 - \frac{dx_j(\theta_{sat,j} - \theta_{r,j})}{\sigma\Delta t} \tag{A.35}$$

$$d_j = \left.\frac{\partial q_{w,j-1}}{\partial T_j}\right|^0 - \left.\frac{\partial q_{w,j}}{\partial T_j}\right|^0 \tag{A.36}$$

$$e_j = \left.\frac{-\partial q_{w,j}}{\partial S_{j+1}}\right|^0 \tag{A.37}$$

$$f_j = \left.\frac{-\partial q_{w,j}}{\partial T_{j+1}}\right|^0 \tag{A.38}$$

$$g_j = -(q^0_{w,j-1} - q^0_{w,j})/\sigma + r_{ex,j}dx_j/\sigma \tag{A.39}$$

Similarly, the discretised conservation equation for heat is:

$$\frac{c_{soil,j}dx_j\Delta T_j}{\Delta t} = q^\sigma_{H,j} - 1 - q^\sigma_{H,j} \tag{A.40}$$

with the linearised heat fluxes:

$$q^\sigma_{H,j} = q^0_{H,j} + \sigma\left(\left.\frac{\partial q_{H,j}}{\partial S_j}\right|^0\Delta S_j + \left.\frac{\partial q_{H,j}}{\partial S_{j+1}}\right|^0\Delta S_{j+1}\left.\frac{\partial q_{H,j}}{\partial T_j}\right|^0\Delta T_j + \left.\frac{\partial q_{H,j}}{\partial T_{j+1}}\right|^0\Delta T_{j+1}\right), \quad j = 1,\ldots,n-1 \tag{A.41}$$

Substituting Eq. (A.41) into (A.40) leads to another set of n linear equations:

$$a_{H,j}\Delta S_{j-1} + b_{H,j}\Delta T_{j-1} + c_{H,j}\Delta S_j + d_{H,j}\Delta T_j + e_{H,j}\Delta S_{j+1} + f_{H,j}\Delta T_{j+1} = g_{H,j}, \quad j = 1,\ldots,n \tag{A.42}$$

with

$$a_{H,j} = \left.\frac{\partial q_{H,j-1}}{\partial S_{j-1}}\right|^0 \tag{A.43}$$

$$b_{H,j} = \left.\frac{\partial q_{H,j-1}}{\partial T_{j-1}}\right|^0 \tag{A.44}$$

$$c_{H,j} = \left.\frac{\partial q_{H,j-1}}{\partial S_j}\right|^0 - \left.\frac{\partial q_{H,j}}{\partial S_j}\right|^0 \tag{A.45}$$

$$d_{H,j} = \left.\frac{\partial q_{H,j-1}}{\partial T_j}\right|^0 - \left.\frac{\partial q_{H,j}}{\partial T_j}\right|^0 - \frac{c_{soil}dx_j}{\sigma\Delta t} \tag{A.46}$$

$$e_{H,j} = \left.\frac{-\partial q_{H,j}}{\partial S_{j+1}}\right|^0 \tag{A.47}$$

$$f_{H,j} = \left.\frac{-\partial q_{H,j}}{\partial T_{j+1}}\right|^0 \tag{A.48}$$

$$g_{H,j} = -(q^0_{H,j-1} - q^0_{H,j})/\sigma \tag{A.49}$$

The two sets of linear equations can be written in the form of a sparse matrix equation:

$$\begin{pmatrix}
c_1 & d_1 & e_1 & f_1 & 0 & 0 & 0 & 0 & \cdots & 0 & 0 & 0 & 0 & 0 & 0 & 0 & 0 \\
c_{H,1} & d_{H,1} & e_{H,1} & f_{H,1} & 0 & 0 & 0 & 0 & \cdots & 0 & 0 & 0 & 0 & 0 & 0 & 0 & 0 \\
a_2 & b_2 & c_2 & d_2 & e_2 & f_2 & 0 & 0 & \cdots & 0 & 0 & 0 & 0 & 0 & 0 & 0 & 0 \\
a_{H,2} & b_{H,2} & c_{H,2} & d_{H,2} & e_{H,2} & f_{H,2} & 0 & 0 & \cdots & 0 & 0 & 0 & 0 & 0 & 0 & 0 & 0 \\
0 & 0 & a_3 & b_3 & c_3 & d_3 & e_3 & f_3 & \cdots & 0 & 0 & 0 & 0 & 0 & 0 & 0 & 0 \\
0 & 0 & a_{H,3} & b_{H,3} & c_{H,3} & d_{H,3} & e_{H,3} & f_{H,3} & \cdots & 0 & 0 & 0 & 0 & 0 & 0 & 0 & 0 \\
0 & 0 & 0 & 0 & a_4 & b_4 & c_4 & d_4 & \cdots & 0 & 0 & 0 & 0 & 0 & 0 & 0 & 0 \\
0 & 0 & 0 & 0 & a_{H,4} & b_{H,4} & c_{H,4} & d_{H,4} & \cdots & 0 & 0 & 0 & 0 & 0 & 0 & 0 & 0 \\
\vdots & \vdots & \vdots & \vdots & \vdots & \vdots & \vdots & \vdots & \ddots & \vdots & \vdots & \vdots & \vdots & \vdots & \vdots & \vdots & \vdots \\
0 & 0 & 0 & 0 & 0 & 0 & 0 & 0 & \cdots & a_{n-3} & b_{n-3} & c_{n-3} & d_{n-3} & e_{n-3} & f_{n-3} & 0 & 0 \\
0 & 0 & 0 & 0 & 0 & 0 & 0 & 0 & \cdots & a_{H,n-3} & b_{H,n-3} & c_{H,n-3} & d_{H,n-3} & e_{H,n-3} & f_{H,n-3} & 0 & 0 \\
0 & 0 & 0 & 0 & 0 & 0 & 0 & 0 & \cdots & 0 & 0 & a_{n-2} & b_{n-2} & c_{n-2} & d_{n-2} & e_{n-2} & f_{n-2} \\
0 & 0 & 0 & 0 & 0 & 0 & 0 & 0 & \cdots & 0 & 0 & a_{H,n-2} & b_{H,n-2} & c_{H,n-2} & d_{H,n-2} & e_{H,n-2} & f_{H,n-2} \\
0 & 0 & 0 & 0 & 0 & 0 & 0 & 0 & \cdots & 0 & 0 & 0 & 0 & a_{n-1} & b_{n-1} & c_{n-1} & d_{n-1} \\
0 & 0 & 0 & 0 & 0 & 0 & 0 & 0 & \cdots & 0 & 0 & 0 & 0 & a_{H,n-1} & b_{H,n-1} & c_{H,n-1} & d_{H,n-1} \\
0 & 0 & 0 & 0 & 0 & 0 & 0 & 0 & \cdots & 0 & 0 & 0 & 0 & 0 & 0 & a_n & b_n \\
0 & 0 & 0 & 0 & 0 & 0 & 0 & 0 & \cdots & 0 & 0 & 0 & 0 & 0 & 0 & a_{H,n} & b_{H,n}
\end{pmatrix}
\begin{pmatrix}
\Delta y_1 \\ \Delta T_1 \\ \Delta y_2 \\ \Delta T_2 \\ \Delta y_3 \\ \Delta T_3 \\ \Delta y_4 \\ \Delta T_4 \\ \vdots \\ \Delta y_{n-3} \\ \Delta T_{n-3} \\ \Delta y_{n-2} \\ \Delta T_{n-2} \\ \Delta y_{n-1} \\ \Delta T_{n-1} \\ \Delta y_n \\ \Delta T_n
\end{pmatrix}
=
\begin{pmatrix}
g_1 \\ g_{H,1} \\ g_2 \\ g_{H,2} \\ g_3 \\ g_{H,3} \\ g_4 \\ g_{H,4} \\ \vdots \\ g_{n-3} \\ g_{H,n-3} \\ g_{n-2} \\ g_{H,n-2} \\ g_{n-1} \\ g_{H,n-1} \\ g_n \\ g_{H,n}
\end{pmatrix} \tag{A.50}$$

the solution of which yields $\Delta y = \Delta S$ and ΔT for each of the n layers, if the layers are unsaturated. It yields $\Delta y = \Delta\phi$ and ΔT if the layers are saturated: see Section on Saturation below.

Partial derivatives in Eq. (A.31) are obtained by partial differentiation of:

$$q_{w,j} = \frac{\phi_{l,j-1} - \phi_{l,j}}{dz_j} + \overline{k_{v,h}}\frac{\phi_{v,j-1} - \phi_{v,j}}{dz_j} + wK_{j-1} + (1-w)K_j + \overline{k_{v,T}}\frac{T_{j-1} - T_j}{dz_j} \tag{A.51}$$

where the weight, w, is calculated so that $q_{w,j}$ is zero when h_{j-1} is equal to $h_j - dz_j$ (Ross, 2003). dz_j is the distance between layer

mid-points, except for the top and bottom boundaries, for which dz_j is half of the top/bottom layer thickness. Similarly, partial derivatives in Eq. (A.41) are obtained from partial differentiation of:

$$q_{H,j} = \rho\lambda_E\overline{k_{vap,h}}\left(\frac{\phi_{v,j-1}-\phi_{v,j}}{dz_j}\right) + \left(\rho\lambda_E\overline{k_{vap,h}} + \overline{k_H}\right)\frac{(T_{j-1}-T_j)}{dz_j} \tag{A.52}$$

In Eqs. (A.51) and (A.52), the over-bars denote weighted mean values of variables in layers $j-1$ and j, with weights given by dx_{j-1} and dx_j.

A.3. Saturation

If any layer is saturated, then the change in stored water in that layer is zero, and the moisture balance is:

$$0 = q^{\sigma}_{w,j-1} - q^{\sigma}_{w,j} - r_{ex,j} \tag{A.53}$$

Thus instead of solving for ΔS_j, we solve for $\Delta\phi_j$, replacing S_j by ϕ_j in Eqs. (A.32) and (A.42), and setting the third term in c_j to zero. A saturated layer becomes unsaturated when the matric flux potential drops below its saturated value. For the purpose of constructing and solving the sparse matrix, we use a single moisture variable, Δy_j, which is set to ΔS_j for unsaturated layers and $\Delta\phi_j$ for saturated layers.

A.4. Infiltration, ponding and runoff

In the absence of ponding or litter, infiltration (as required for Eq. (A.30)) is the precipitation rate minus the evaporation rate:

$$q_{w,0} = q_{prec} - q_{evap} \tag{A.54}$$

(Formulations for infiltration in the presence of ponding and litter are presented later (Eqs. (A.55) and (A.115)).) The heat flux into the top of the soil column (as required for Eq. (A.40)) is then:$q_{H,0} = G$. Both $q^0_{evap}$and G^0 are calculated from the coupled moisture/energy conservation equations at the surface.

Ponding occurs if $\phi_{l,1} \geqslant \phi_l(h=0)$. Then infiltration is:

$$q_{w,0} = \frac{K_{sat}(h_p - h_e)}{h_p/2 + dx_1/2} + K_{sat} \tag{A.55}$$

and

$$q_{H,0} = \frac{\overline{k_H}(T_P - T_1)}{h_p/2 + dx_1/2} \tag{A.56}$$

If ponding occurs, we enlarge our sparse matrix by two rows and two columns and solve for the changes in pond height (h_0) and pond temperature (T_0) over the time step. The discretised conservation equations for the pond height and pond temperature are:

$$\frac{\Delta h_P}{\Delta t} = (q_{prec} - q_{evap}) - q^0_{w,0} - \sigma\frac{\partial q_{w,0}}{\partial h_0}\Delta h_P \tag{A.57}$$

$$\frac{c_w h_P \Delta T_P}{\Delta t} = (G - q^0_{H,0}) - \sigma\left(\frac{\partial q_{H,0}}{\partial h_0}\Delta h_P + \frac{\partial q_{H,0}}{\partial T_0}\Delta T_P + \frac{\partial q_{H,0}}{\partial T_1}\Delta T_1\right) \tag{A.58}$$

The coefficients for the additional rows in the sparse matrix are:

$$c_0 = \left.\frac{\partial q_{w,0}}{\partial h_0}\right|^0 - \frac{1}{\sigma\Delta t} \tag{A.59}$$

$$g_0 = -\frac{q_{prec} - q_{evap} - q^0_{w,0}}{\sigma} \tag{A.60}$$

$$d_0 = e_0 = f_0 = 0 \tag{A.61}$$

$$c_{H,0} = -\left.\frac{\partial q_{H,0}}{\partial h_0}\right|^0 \tag{A.62}$$

$$d_{H,0} = -\left.\frac{\partial q_{H,0}}{\partial T_0}\right|^0 - \frac{c_w h_0}{\sigma\Delta t} \tag{A.63}$$

$$C_{H,0} = 0 \tag{A.64}$$

$$f_{H,0} = \left.\frac{-\partial q_{H,0}}{\partial T_1}\right|^0 \tag{A.65}$$

$$g_{H,0} = -(G - q^0_{H,0})/\sigma \tag{A.66}$$

Runoff occurs when the pond height exceed its user-defined maximum value, $h_{P,max}$:

$$q_{runoff} = \begin{cases} q_{prec} - q_{evap} - q_{w,0}, & h_P > h_{P,\max} \\ 0, & h_P \leqslant h_{P,\max} \end{cases} \tag{A.67}$$

When $h_P > h_{P,\max}$, h_P remains constant for the duration of the timestep and we do not solve Eq. (A.57), but retain Eq. (A.58), so that the number of rows and columns in the sparse matrix is $2n+1$.

A.5. Litter

The optional litter layer is characterised by the following parameters: thickness dx_L; volumetric heat capacity of dry litter $c_{L,d}$, saturated moisture content $\theta_{sat,L}$, dry bulk density ρ_{bL}, pressure head at saturation h_{eL}. The hydraulic conductivity of the litter is set to zero and therefore there is no movement of liquid water within the litter by suction. Downward movement of liquid water from the litter layer to the soil column is possible by drainage which can occur when the litter is saturated (Eq. (A.68)). While the litter is unsaturated, there is no drainage of liquid water from the litter to the soil. Once the litter is saturated, all the available liquid water drains to the soil and is available for infiltration.

$$q_d = \begin{cases} q_{prec} - q_{evap}, & \theta_L = \theta_{sat,L} \\ 0, & \theta_L < \theta_{sat,L} \end{cases} \tag{A.68}$$

Pressure head is related to litter moisture content by (Ogée and Brunet, 2002):

$$h_L = h_{e,L}\left(\frac{\rho}{\rho_{bL}}\theta_L\right)^{-1/\lambda_L} \tag{A.69}$$

which is related to relative humidity by the Kelvin equation (Eq. (A.14)). Following measurements of Myrold et al. (1981), we assume parameter values of $h_{e,L} = -35.0$ m, $\lambda_L = 0.42$. These values are considered as standard for dead organic material (Ogée and Brunet, 2002). $h_{e,L}$ is highly negative because it is associated with water which is strongly adsorbed within the litter particles.

Vapour diffusivity within the litter is estimated using the empirical formulation of Matthews (2006):

$$D_T(z_L) = D_{T0}\exp\left\{\chi\left(\frac{z_L}{dx_L} - 1\right)\right\} \tag{A.70}$$

$$D_{T0} = D_{T0,a}\exp(UD_{T0,b}) \tag{A.71}$$

$$\chi = \chi_a + U\chi_b \tag{A.72}$$

where z_L is the depth within the litter (set here to $0.5dx_L$); U is windspeed 10 cm above the litter surface and χ_a, χ_b, $D_{T0,a}$ and $D_{T0,b}$ are empirical coefficients with respective values of 2.08, 2.38 m s^{-1}, 2×10^{-5} m^2 s^{-1}, 2.60 m^{-1} s.

Heat conductivity of the litter layer is also taken from Matthews (2006):

$$k_{H,L} = 0.2 + 0.14\theta_L\frac{\rho}{\rho_{bL}} \tag{A.73}$$

Heat capacity is related to moisture content:

$$c_L = c_{L,d} + c_w\theta_L \tag{A.74}$$

Wit c_w the volumetric heat capacity of liquid water (4.18×10^6 J m^{-3} K^{-1}) and $c_{L,d}$ is the volumetric heat capacity of dry litter ($1932\rho_{b,L}$ J m^{-3} K^{-1}).

When a litter layer is present, we require two additional linear equations ((A.75) and (A.76)) for the moisture and energy balances on the litter layer. Moisture content of the litter changes in response to precipitation, evaporation from the litter, water flux at the top of the soil column (in absence of drainage) and drainage (Eq. (A.68)):

$$\frac{dx_L\Delta S_L\theta_{sat,L}}{\Delta t} = q_{prec} - q_{evap} - q_{w,0} - q_d \tag{A.75}$$

The heat content of the litter changes in response to the heat flux at the litter surface and the heat flux at the soil/litter interface:

$$\frac{c_L dx_L\Delta T_L}{\Delta t} = G_0 - q_{H,0} \tag{A.76}$$

and hence two additional rows and columns in our sparse matrix equation, with additional variables being the change in litter temperature and degree of litter saturation: ΔT_L and ΔS_L. Expanding the fluxes in Eqs. (A.75) and (A.76) as:

$$q^{\sigma}_{w,0} = q^0_{w,0} + \sigma\left(\left.\frac{\partial q_{w,0}}{\partial S_L}\right|^0\Delta S_L + \left.\frac{\partial q_{w,0}}{\partial S_1}\right|^0\Delta S_1 + \left.\frac{\partial q_{w,0}}{\partial T_L}\right|^0\Delta T_L + \left.\frac{\partial q_{w,0}}{\partial T_1}\right|^0\Delta T_1\right) \tag{A.77}$$

$$q^{\sigma}_{evap,0} = q^0_{evap,0} + \sigma\left(\left.\frac{\partial q_{evap,0}}{\partial S_L}\right|^0\Delta S_L + \left.\frac{\partial q_{evap,0}}{\partial T_L}\right|^0\Delta T_L\right) \tag{A.78}$$

$$q^{\sigma}_{H,0} = q^0_{H,0} + \sigma\left(\left.\frac{\partial q_{H,0}}{\partial S_L}\right|^0\Delta S_L + \left.\frac{\partial q_{H,0}}{\partial S_1}\right|^0\Delta S_1 + \left.\frac{\partial q_{H,0}}{\partial T_L}\right|^0\Delta T_L + \left.\frac{\partial q_{H,0}}{\partial T_1}\right|^0\Delta T_1\right) \tag{A.79}$$

$$G^{\sigma} = G^0 + \sigma\left(\left.\frac{\partial G}{\partial S_L}\right|^0\Delta S_L + \left.\frac{\partial G}{\partial T_L}\right|^0\Delta T_L\right) \tag{A.80}$$

leads to the following coefficients in the additional matrix rows:

$$c_0 = -\frac{dx_L\theta_{sat,L}}{\sigma\Delta t} - \left.\frac{\partial q_{evap}}{\partial S_L}\right|^0 - \left.\frac{\partial q_{w,0}}{\partial S_L}\right|^0 \tag{A.81}$$

$$d_0 = -\left.\frac{\partial q_{evap}}{\partial T_L}\right|^0 - \left.\frac{\partial q_{w,0}}{\partial T_L}\right|^0 \tag{A.82}$$

$$e_0 = -\left.\frac{\partial q_{w,0}}{\partial S_1}\right|^0 \tag{A.83}$$

$$f_0 = -\left.\frac{\partial q_{w,0}}{\partial T_1}\right|^0 \tag{A.84}$$

$$g_0 = -\frac{(q_{prec} - q^0_{evap} - q^0_{w,0} - q_d)}{\sigma} \tag{A.85}$$

$$c_{H,0} = \left.\frac{\partial G}{\partial S_L}\right|^0 - \left.\frac{\partial q_{H,0}}{\partial S_L}\right|^0 \tag{A.86}$$

$$d_{H,0} = \frac{-c_L dx_L}{\sigma\Delta t} + \left.\frac{\partial G}{\partial T_L}\right|^0 - \left.\frac{\partial q_{H,0}}{\partial T_L}\right|^0 \tag{A.87}$$

$$e_{H,0} = -\left.\frac{\partial q_{H,0}}{\partial S_L}\right|^0 \tag{A.88}$$

$$f_{H,0} = -\left.\frac{\partial q_{H,0}}{\partial T_L}\right|^0 \tag{A.89}$$

$$g_{H,0} = -\frac{G^0 - q^0_{H,0}}{\sigma} \tag{A.90}$$

We note here that the inclusion of a litter layer using the above equations leads to a significant increase in computation time because the linear approximations of Eqs. (A.77)–(A.80) are only valid for small changes in temperature and moisture content and because litter temperature in particular tends to change rapidly with time. This is because the litter has a low heat capacity compared to soil, and its temperature is therefore very sensitive to hourly changes in meteorological forcing variables, particularly radiation and air temperature. The increase in computation time can be lessened by rewriting Eqs. (A.77)–(A.80) as expansions about $T_L^{\sigma,approx}$ instead of T_L^0:

$$q^{\sigma}_{w,0} = q^0_{w,0} + \sigma\left(\left.\frac{\partial q_{w,0}}{\partial S_L}\right|^0\Delta S_L + \left.\frac{\partial q_{w,0}}{\partial S_1}\right|^0\Delta S_1 + \left.\frac{\partial q_{w,0}}{\partial T_L}\right|^0\left(\Delta T_L + T^0_L - T^{\sigma,approx}_L\right) + \left.\frac{\partial q_{w,0}}{\partial T_1}\right|^0\Delta T_1\right) \tag{A.91}$$

$$q^{\sigma}_{evap,0} = q^0_{evap,0} + \sigma\left(\left.\frac{\partial q_{evap,0}}{\partial S_L}\right|^0\Delta S_L + \left.\frac{\partial q_{evap,0}}{\partial T_L}\right|^0\left(\Delta T_L + T^0_L - T^{\sigma,approx}_L\right)\right) \tag{A.92}$$

$$q^{\sigma}_{H,0} = q^0_{H,0} + \sigma\left(\left.\frac{\partial q_{H,0}}{\partial S_L}\right|^0\Delta S_L + \left.\frac{\partial q_{H,0}}{\partial S_1}\right|^0\Delta S_1 + \left.\frac{\partial q_{H,0}}{\partial T_L}\right|^0\left(\Delta T_L + T^0_L - T^{\sigma,approx}_L\right)_L + \left.\frac{\partial q_{H,0}}{\partial T_1}\right|^0\Delta T_1\right) \tag{A.93}$$

$$G^{\sigma} = G^0 + \sigma\left(\left.\frac{\partial G}{\partial S_L}\right|^0\Delta S_L + \left.\frac{\partial G}{\partial T_L}\right|^0\left(\Delta T_L + T^0_L - T^{\sigma,approx}_L\right)\right) \tag{A.94}$$

where T_L^0 is the litter temperature at the end of the previous time-step and $T_L^{\sigma,approx}$ is an approximation to the litter temperature midway through the current time-step which accounts for the significant influences of updated R_{net} and T_a. It is estimated by equating heat fluxes at the litter/air and soil/air interfaces, assuming: (i) a uniform litter temperature within and at both lower and upper boundaries of the litter layer; (ii) latent heat flux and soil temperature are equal to those of the previous time-step:

$$\frac{T^{\sigma,approx}_L - T^0_{soil,1}}{dx_L/2/k_{th,L} + dx_1/2/k_{th,1}} = R_{net} - \lambda E^0 + (T_a - T^{\sigma,approx}_L)\rho c_p/r_{bh} \tag{A.95}$$

Initial flux estimates at the litter/air and soil/litter interfaces ($q^0_{w,0}; q^0_{evap,0}; q^0_{H,0}G^0$), and their partial derivatives are made using $T_L^{\sigma,approx}$. The coefficients in the top two matrix rows remain the same, except for g_0 and $g_{H,0}$ which become:

$$g_0 = -\frac{(q_{prec} - q^0_{evap} - q^0_{w,0} - q_d)}{\sigma} - \left(T^0_L - T^{\sigma,approx}_L\right)\left(\left.\frac{\partial q_{evap}}{\partial T_L}\right|^0 + \left.\frac{\partial q_{w,0}}{\partial T_L}\right|^0\right) \tag{A.96}$$

$$g_{H,0} = -\frac{G^0 - q^0_{H,0}}{\sigma} - (T^0_L - T^{\sigma,approx}_L)\left(-\left.\frac{\partial G}{\partial T_L}\right|^0 + \left.\frac{\partial q_{H,0}}{\partial T_L}\right|^0\right) \tag{A.97}$$

When litter and pond water are present simultaneously, they are assumed to occupy the same vertical layer. In the presence of a pond, S_L is held constant at its saturated value and Eq. (A.57) is solved for the change in pond height. A single temperature, T_L, is assigned to the pond and litter and Eq. (A.76) is modified to account for the heat capacity of the pond water:

$$\frac{(c_L dx_L + c_w h_P)\Delta T_L}{\Delta t} = G_0 - q_{H,0} \tag{A.98}$$

The heat and moisture fluxes (at the beginning of the time step) at the air/litter and litter/soil interfaces are determined by solving

the coupled moisture and energy conservation equations at these interfaces, as described below. Partial derivatives of these fluxes were evaluated numerically by revaluating the fluxes using perturbed values of temperature and moisture variables in the litter and top soil layer.

A.6. Upper boundary condition: no ponding or litter

In the absence of ponding or litter, the surface temperature (T_s) and relative humidity ($h_{r,s}$) are evaluated by solving the coupled equations for moisture and energy conservation at the soil/air interface:

$$\frac{1}{r_{bw}}[h_{r,s}(c_{v,sat}(T_1)+s(T_1)(T_s-T_1))-c_{v,a}] = \frac{D_{v,1}}{dx_1/2}c_{v,sat}(T_1)(h_{r,1}-h_{r,s})+\frac{D_{v,1}}{dx_1/2}s(T_1)h_{r,1}(T_1-T_s) + \left[\frac{(\phi_l(h_{r,1})-\phi_l(h_{r,s}))}{dx_1/2}-K_1\right] \quad (A.99)$$

$$R_{net}=\frac{\rho_a c_p}{r_{bh}}(T_s-T_a)+\frac{\rho\lambda_e}{r_{bw}}[h_{r,s}(c_{v,sat}(T_1)+s(T_1)(T_s-T_1))-c_{v,a}] - \frac{k_{H,1}}{dx_1/2}(T_1-T_s) \quad (A.100)$$

In Eq. (A.99), the left hand side is the water vapour flux from the surface to the atmosphere. Note here that, $c_{v,s}$ is approximated as:

$$c_{v,s}\simeq h_{r,s}(c_{v,sat}(T_1)+s(T_1)(T_s-T_1)) \quad (A.101)$$

On the right hand side of Eq. (A.99), the first and second terms sum to give the vapour flux from the centre of the top soil layer to the soil surface ($-q_{v,s}$). The first term is the component of the vapour flux driven by a moisture gradient, and the second is the component driven by a temperature gradient. The third term is the liquid flux from the centre of the top soil layer to the soil surface ($-q_{l,s}$), and consists of a component due to the soil moisture potential gradient, and a gravitational flux. Since Eqs. (A.99) and (A.100) are non-linear in T_s and $h_{r,s}$, we use a numerical root-finding method to solve for these variables. These in turn allow us to evaluate surface evaporation; liquid flux at the surface; vapour flux at the surface; surface sensible heat flux, surface latent heat flux and heat flux into the soil respectively:

$$q_{evap}=\frac{1}{r_{bw}}[h_{r,s}(c_{v,sat}(T_1)+s(T_1)(T_s-T_1))-c_{v,a}] \quad (A.102)$$

$$q_{v,s}=-\frac{D_{v,1}}{\Delta x_1/2}c_{v,sat}(T_1)(h_{r,1}-h_{r,s})-\frac{D_{v,1}}{\Delta x_1/2}s(T_1)h_{r,1}(T_1-T_s) \quad (A.103)$$

$$q_{l,s}=-\left[\frac{(\phi_l(h_{r,1})-\phi_l(h_{r,s}))}{\Delta x_1/2}-K_1\right] \quad (A.104)$$

$$H=\frac{\rho_a c_p}{r_{rc}}(T_s-T_a) \quad (A.105)$$

$$\lambda_E E=\lambda_E\rho q_{evap} \quad (A.106)$$

$$G=-\frac{k_{H,1}}{dx_1/2}(T_1-T_s) \quad (A.107)$$

A.7. Upper boundary condition: litter (no pond)

In the presence of litter and no pond, the moisture and energy conservation equations at the air/litter interface are:

$$\frac{1}{r_{bw}}[h_{r,s}(c_{v,sat}(T_L)+s(T_L)(T_s-T_L))-c_{v,a}] = \frac{D_{v,L}}{\Delta x_L/2}c_{v,sat}(T_L)(h_{r,L}-h_{r,s})+\frac{D_{v,L}}{\Delta x_L/2}s(T_L)h_{r,L}(T_L-T_s) \quad (A.108)$$

$$R_{net}=\frac{\rho_a c_p}{r_{rc}}(T_s-T_a)+\frac{\rho\lambda_e}{r_{bw}}[h_{r,s}(c_{v,sat}(T_L)+s(T_L)(T_s-T_L))-c_{v,a}] - \frac{k_{th,L}}{dx_L/2}(T_L-T_s) \quad (A.109)$$

Eqs. (A.108) and (A.109) are solved simultaneously for T_s and $h_{r,s}$ which are then used to calculate the surface evaporation and components of the surface energy balance.

And at the litter/soil interface, the moisture and energy conservation equations are:

$$\frac{D_{v,L}}{dx_L/2}[h_{r,SL}(c_{v,sat}(T_1)+s(T_1)(T_{SL}-T_1))-c_{v,L}] = \frac{D_{v,1}}{dx_1/2}c_{v,sat}(T_1)(h_{r,1}-h_{r,SL})+\frac{D_{v,1}}{dx_1/2}s(T_1)h_{r,1}(T_1-T_{SL}) + \left[\frac{(\phi_l(h_{r,1})-\phi_l(h_{r,SL}))}{dx_1/2}-K_1\right] \quad (A.110)$$

$$0=\frac{k_{H,L}}{dx_L/2}(T_{SL}-T_L)+\frac{\lambda_e D_{v,L}}{dx_L/2}[h_{r,SL}(c_{v,sat}(T_L)+s(T_L)(T_{SL}-T_L))-c_{v,L}] - \frac{k_{H,1}}{dx_1/2}(T_1-T_{SL}) \quad (A.111)$$

Eqs. (A.110) and (A.111) are solved simultaneously for T_{SL} and $h_{r,SL}$. These in turn allow us to evaluate evaporation from the soil to the litter; liquid flux at the soil surface; vapour flux at the soil surface; water flux into the soil column and heat flux into the soil column respectively:

$$q_{evap,L}=\frac{D_{v,L}}{dx_L/2}[h_{r,sL}(c_{v,sat}(T_1)+s(T_1)(T_{sL}-T_1))-c_{v,L}] \quad (A.112)$$

$$q_{l,SL}=-\left[\frac{(\phi_l(h_{r,1})-\phi_l(h_{r,SL}))}{dx_1/2}-K_1\right] \quad (A.113)$$

$$q_{v,SL}=-\frac{D_{v,1}}{dx_1/2}c_{v,sat}(T_1)(h_{r,1}-h_{r,sL})-\frac{D_{v,1}}{dx_1/2}s(T_1)h_{r,1}(T_1-T_{SL}) \quad (A.114)$$

$$q_{w,0}=q_{l,SL}+q_{v,SL} \quad (A.115)$$

$$q_{H,0}=-\frac{k_{H,1}}{dx_1/2}(T_1-T_{SL}) \quad (A.116)$$

A.8. Upper boundary condition: ponding

In the presence of a pond, the relative humidity at the pond surface is one, and the surface temperature is estimated by solving the following energy conservation equation:

$$R_{net}=\frac{\rho_a c_p}{r_{rc}}(T_s-T_a)+\frac{\rho\lambda_e}{r_{bw}}[(c_{v,sat}(T_L)+s(T_1)(T_s-T_L))-c_{v,a}] - \frac{k_w}{h_P/2}(T_L-T_s) \quad (A.117)$$

In Eq. (A.117), the three terms on the right hand side are H, $\lambda_E E$ and G. q_{evap} is related to $\lambda_E E$ by Eq. (A.106).

A.9. Lower boundary conditions

The lower boundary conditions are free drainage ($q_{w,n}=K_n$) and zero heat flux ($q_{H,n}=0$).

Appendix B. Model for stable isotope transport

B.1. Fluxes of HDO or $H_2{}^{18}O$ within the soil column

The one-dimensional conservation equation for the minor isotopologue (HDO or $H_2{}^{18}O$) is:

$$\frac{\partial}{\partial t}\{c_l^i[\theta_l+\alpha^+c_v(\theta_{sat}-\theta_l)]\}=-\frac{\partial}{\partial z}(q_l^i+q_v^i)-c_l^i r_{ex} \tag{B.1}$$

The liquid-phase flux of the minor isotopologue is the sum of advective and diffusive components:

$$q_l^i=c_l^i q_l-D_l^i\frac{dc_l^i}{dz} \tag{B.2}$$

Similarly to Eq. (A.9), we write the vapour-phase flux of the minor isotopologue as:

$$q_v^i=-D_v^i\frac{dc_v^i}{dz}=-D_v^i\frac{d(\alpha^+c_l^ic_v)}{dz}=-D_v^i\alpha^+c_l^i\frac{dc_v}{dz}-D_v^ic_v\left(\alpha^+\frac{dc_l^i}{dz}+c_l^i\frac{d\alpha^+}{dz}\right) \tag{B.3}$$

Substituting Eq. (A.12) into Eq. (B.3), we obtain

$$q_v^i=\alpha_{k,diff}\alpha^+c_l^iq_v-D_v^ic_v\alpha^+\frac{dc_l^i}{dz}-D_v^ic_vc_l^i\frac{d\alpha^+}{dz} \tag{B.4}$$

where

$$\alpha_{k,diff}=\frac{D_v^i}{D_v} \tag{B.5}$$

The terms in Eq. (B.4) are: (i) the advective flux of the minor isotopologue in the vapour-phase; (ii) the component of the vapour diffusive flux due to the vertical concentration gradient in the liquid phase; (iii) the component of the vapour diffusive flux due to the vertical gradient in the equilibrium fractionation factor (which is dependent on soil temperature).

Substituting Eqs. (B.3) and (B.4) into (B.1), and noting that $\theta=S(\theta_{sat}-\theta_r)+\theta_r$, the conservation equation becomes:

$$\begin{aligned}&\frac{\partial}{\partial t}\{c_l^i[S(\theta_{sat}-\theta_r)+\theta_r+\alpha^+c_v(\theta_{sat}-\theta_r)(1-S)]\}\\&\quad=-\frac{\partial}{\partial z}\left(c_l^iq_l-D_l^i\frac{dc_l^i}{dz}+\alpha_{k,diff}\alpha^+c_l^iq_v-D_v^ic_v\alpha^+\frac{dc_l^i}{dz}-D_v^ic_vc_l^i\frac{d\alpha^+}{dz}\right)\\&\qquad-c_l^ir_{ex}\end{aligned} \tag{B.6}$$

B.2. Discretisation

We rewrite Eq. (B.6) in discrete form as:

$$\begin{aligned}&\frac{\theta_{sat,j}dx_j}{\Delta t}\left(c_{l,j}^i\Delta S_{eff,j}+S_{eff,j}\Delta c_{l,j}^i\right)\\&=q_{l,j-1}^\sigma\left(\overline{c_{q_l,j-1}^i}+\sigma\Delta c_{l,j-1}^i\frac{\partial\overline{c_{q_l,j-1}^i}}{\partial c_{l,j-1}^i}+\sigma\Delta c_{l,j}^i\frac{\partial\overline{c_{q_l,j-1}^i}}{\partial c_{l,j}^i}\right)\\&\quad-q_{l,j}^\sigma\left(\overline{c_{q_l,j}^i}+\sigma\Delta c_{l,j}^i\frac{\partial\overline{c_{q_l,j}^i}}{\partial c_{q_l,j}^i}+\sigma\Delta c_{l,j+1}^i\frac{\partial\overline{c_{q_l,j}^i}}{\partial c_{q_l,j+1}^i}\right)\\&\quad+q_{v,j-1}^\sigma\overline{\alpha_{j-1}^+}\alpha_{k,diff}\left(\overline{c_{q_v,j-1}^i}+\sigma\Delta c_{l,j-1}^i\frac{\partial\overline{c_{q_v,j-1}^i}}{\partial c_{l,j-1}^i}+\sigma\Delta c_{l,j}^i\frac{\partial\overline{c_{q_v,j-1}^i}}{\partial c_{l,j}^i}\right)\\&\quad-q_{v,j}^\sigma\overline{\alpha_j^+}\alpha_{k,diff}\left(\overline{c_{q_v,j}^i}+\sigma\Delta c_{l,j}^i\frac{\partial\overline{c_{q_v,j}^i}}{\partial c_{l,j}^i}+\sigma\Delta c_{l,j+1}^i\frac{\partial\overline{c_{q_v,j}^i}}{\partial c_{l,j+1}^i}\right)\\&\quad+\frac{\overline{D_{l,j-1}^i}}{dz_{j-1}}\left((c_{l,j-1}^i+\sigma\Delta c_{l,j-1}^i)-(c_{l,j}^i+\sigma\Delta c_{l,j}^i)\right)-\frac{\overline{D_{l,j}^i}}{dz_j}((c_{l,j}^i+\sigma\Delta c_{l,j}^i)\\&\quad-(c_{l,j+1}^i+\sigma\Delta c_{l,j+1}^i))+\frac{\overline{D_{v,j-1}^ic_{v,j-1}\alpha_{j-1}^+}}{dz_{j-1}}((c_{l,j-1}^i+\sigma\Delta c_{l,j-1}^i)\\&\quad-(c_{l,j}^i+\sigma\Delta c_{l,j}^i))-\frac{\overline{D_{v,j}^ic_{v,j}\alpha_j^+}}{dz_j}((c_{l,j}^i+\sigma\Delta c_{l,j}^i)-(c_{l,j+1}^i+\sigma\Delta c_{l,j+1}^i))\\&\quad-q_{ex,j}(c_{l,j}^i+\sigma\Delta c_{l,j}^i)\end{aligned} \tag{B.7}$$

The left hand side of Eq. (B.7) is the rate of change of storage of the minor isotopologue in the j^{th} layer, with $S_{eff,j}$ and $\Delta S_{eff,j}$ defined as:

$$S_{eff,j}=S_{l,j}^\sigma+c_{v,j}^\sigma\alpha_j^+-c_{v,j}^\sigma S_{l,j}^\sigma\alpha_j^++\theta_{r,j}/(\theta_{sat,j}-\theta_{r,j}) \tag{B.8}$$

$$\Delta S_{eff,j}=\Delta S_{l,j}+\alpha_j^+\Delta c_{v,j}+c_{v,j}^\sigma\Delta\alpha_j^+-(S_{l,j}^\sigma\alpha_j^+\Delta c_{v,j}^+c_{v,j}^\sigma\alpha_j^+\Delta S_{l,j}+c_{v,j}^\sigma S_{l,j}^\sigma\Delta\alpha_j^+) \tag{B.9}$$

The terms on the right hand side of Eq. (B.7) represent: (i) liquid advection from the layer above; (ii) liquid advection to the layer below; (iii) vapour advection from the layer above; (iv) vapour advection to the layer below; (v) liquid diffusion from the layer above; (vi) liquid diffusion to the layer below; (vii) vapour diffusion from the layer above; (viii) vapour diffusion to the layer below; (ix) root extraction. (Isotopic transport due to a vertical gradient in α^+ is negligible and has not been included here.) For the advective terms, the discretisation requires an estimate of the concentration of the isotopologue in the fluid being advected between layers j and $j+1$. For liquid advection, this concentration is defined as:

$$\overline{c_{q_l,j}^i}=w_{l,j}c_{l,j}^i+(1-w_{l,j})c_{l,j+1}^i \tag{B.10}$$

Similarly, for vapour advection:

$$\overline{c_{q_v,j}^i}=w_{v,j}c_{l,j}^i+(1-w_{v,j})c_{l,j+1}^i \tag{B.11}$$

We define the weighting coefficients in Eqs. (B.10) and (B.11) as

$$w_{l,j}=\begin{cases}1, & q_{l,j}\geqslant 0\\ 0, & q_{l,j}<0\end{cases} \tag{B.12}$$

$$w_{v,j}=\begin{cases}1, & q_{vap,j}\geqslant 0\\ 0, & q_{vap,j}<0\end{cases} \tag{B.13}$$

These coefficients produce more stable solutions than $w_{l,j}=w_{v,j}=0.5$, particularly when two or more adjacent soil layers are saturated.

We rewrite Eq. (B.7) in tridiagonal matrix form as:

$$A_j\Delta c_{l,j-1}^i+B_j\Delta c_{l,j}^i+C_j\Delta c_{l,j+1}^i=D_j, j=1,\ldots,n \tag{B.14}$$

and solve for $\Delta c_{l,j}^i(j=1,\ldots,n)$.

The coefficients in Eq. (B.14) are:

$$A_j=q_{l,j-1}^\sigma\frac{\partial\overline{c_{q_l,j-1}^i}}{\partial c_{l,j-1}^i}+q_{v,j-1}^\sigma\overline{\alpha_{j-1}^+}\alpha_{k,diff}\frac{\partial\overline{c_{q_v,j-1}^i}}{\partial c_{l,j-1}^i}+\frac{\overline{D_{l,j-1}^i}}{dz_{j-1}}+\frac{\overline{D_{v,j-1}^ic_{v,j-1}\alpha_{j-1}^+}}{dz_{j-1}} \tag{B.15}$$

$$\begin{aligned}B_j=&-S_{eff,j}\frac{\theta_{sat,j}dx_j}{\sigma\Delta t}+q_{l,j-1}^\sigma\frac{\partial\overline{c_{q_l,j-1}^i}}{\partial c_{l,j}^i}-q_{l,j}^\sigma\frac{\partial\overline{c_{q_l,j}^i}}{\partial c_{q_l,j}^i}\\&+q_{v,j-1}^\sigma\overline{\alpha_{j-1}^+}\alpha_{k,diff}\frac{\partial\overline{c_{q_v,j-1}^i}}{\partial c_{l,j}^i}-q_{v,j}^\sigma\overline{\alpha_j^+}\alpha_{k,diff}\frac{\partial\overline{c_{q_v,j}^i}}{\partial c_{l,j}^i}-\frac{\overline{D_{l,j-1}^i}}{dz_{j-1}}-\frac{\overline{D_{l,j}^i}}{dz_j}\\&-\frac{\overline{D_{v,j-1}^ic_{v,j-1}\alpha_{j-1}^+}}{dz_{j-1}}-\frac{\overline{D_{v,j}^ic_{v,j}\alpha_j^+}}{dz_j}-q_{ex,j}\end{aligned} \tag{B.16}$$

$$C_j=-q_{l,j}^\sigma\frac{\partial\overline{c_{q_l,j}^i}}{\partial c_{q_l,j+1}^i}-q_{v,j}^\sigma\overline{\alpha_j^+}\alpha_{k,diff}\frac{\partial\overline{c_{q_v,j}^i}}{\partial c_{l,j+1}^i}+\frac{\overline{D_{l,j}^i}}{dz_j}+\frac{\overline{D_{v,j}^ic_{v,j}\alpha_j^+}}{dz_j} \tag{B.17}$$

$$\begin{aligned}D_j=&\frac{\theta_{sat,j}dx_j}{\sigma\Delta t}c_{l,j}^i\Delta S_{eff,j}-q_{l,j-1}^\sigma\overline{c_{q_l,j-1}^i}/\sigma+q_{l,j}^\sigma\overline{c_{q_l,j}^i}/\sigma\\&-q_{v,j-1}^\sigma\overline{\alpha_{j-1}^+}\alpha_{k,diff}\overline{c_{q_v,j-1}^i}/\sigma+q_{v,j}^\sigma\overline{\alpha_j^+}\alpha_{k,diff}\overline{c_{q_v,j}^i}/\sigma-\frac{\overline{D_{l,j-1}^i}}{dz_{j-1}}\\&\times(c_{l,j-1}^i-c_{l,j}^i)/\sigma+\frac{\overline{D_{l,j}^i}}{dz_j}(c_{l,j}^i-c_{l,j+1}^i)/\sigma-\frac{\overline{D_{v,j-1}^ic_{v,j-1}\alpha_{j-1}^+}}{dz_{j-1}}\\&\times(c_{l,j-1}^i-c_{l,j}^i)/\sigma+\frac{\overline{D_{v,j}^ic_{v,j}\alpha_j^+}}{dz_j}(c_{l,j}^i-c_{l,j+1}^i)/\sigma+q_{ex,j}c_{l,j}^i/\sigma\end{aligned} \tag{B.18}$$

B.3. Upper boundary condition: no ponding or litter

The flux of the minor isotopologue into the top of the soil column is:

$$q_0^i = c_{prec} q_{prec} - (c_{evap,out} q_{evap,out} - c_{evap,in} q_{evap,in}) \tag{B.19}$$

Net evaporation from the soil surface can be written as:

$$q_{evap} = q_{evap,out} - q_{evap,in} \tag{B.20}$$

with

$$q_{evap,out} = c_{v,s}/r_{bw} \tag{B.21}$$

and

$$q_{evap,in} = c_{v,a}/r_{bw} \tag{B.22}$$

Similarly, the evaporative flux of the minor isotopologue can be written as:

$$q^i_{evap} = q^i_{evap,out} - q^i_{evap,in} = c^i_{evap,out} q_{evap,out} - c^i_{evap,in} q_{evap,in} \tag{B.23}$$

with

$$q^i_{evap,out} = \frac{\alpha_k c^i_{v,s}}{r_{bw}} = \frac{\alpha_k \alpha^+(T_s) c^i_{l,s} c_{v,s}}{r_{bw}} = \alpha_k \alpha^+(T_s) c^i_{l,s} q_{evap,out} \tag{B.24}$$

and

$$q^i_{evap,in} = \frac{\alpha_k c^i_{v,a}}{r_{bw}} = \frac{\alpha_k c_{v,a} \rho R_a M_i/M_w}{r_{bw}} = \alpha_k \rho R_a M_i/M_w q_{evap,in} \tag{B.25}$$

and hence

$$c^i_{evap,out} = \alpha_k \alpha^+(T_s) c^i_{l,s} \tag{B.26}$$

$$c^i_{evap,in} = \alpha_k \rho R_a M_i/M_w \tag{B.27}$$

Similarly to Eq. (A.99), the equation for conservation of the minor isotopologue at the soil/air interface is:

$$\begin{aligned} &\frac{\alpha_k}{r_{bw}}\left[c_{v,s} c^i_{l,s} \alpha^+(T_s) - c^i_{v,a}\right] \\ &\quad = \alpha_{k,diff} \frac{D_{v,1}}{\Delta x_1/2}(c_{v,1}\alpha^+(T_1) c^i_{l,1} - c_{v,s} c^i_{l,s} \alpha^+(T_s)) \\ &\qquad - q_{l,0}(w_s c^i_{l,s} + w_1 c^i_{l,1}) + \frac{D^i_{l,1}}{\Delta x_1/2}(c^i_{l,1} - c^i_{l,s}) \end{aligned} \tag{B.28}$$

Rearranging Eq. (B.28) leads to the following expression for $c^i_{l,s}$, which is required to evaluate $c^i_{evap,out}$:

$$c^i_{l,s} = \frac{\alpha_{k,diff} \frac{D_{v,1}}{\Delta x_1/2} c_{v,1} \alpha^+(T_1) c^i_{l,1} + c^i_{v,a} \alpha_k / r_{bw} - q_{l,0} c^i_{l,1} w_1 + \frac{D^i_{l,1}}{\Delta x_1/2} c^i_{l,1}}{\alpha^+(T_s)\alpha_k c_{v,s}/r_{bw} + q_{l,0} w_s + \alpha^+(T_s)\alpha_{k,diff} c_{v,s} \frac{D_{v,1}}{\Delta x_1/2} + \frac{D^i_{l,1}}{\Delta x_1/2}} \tag{B.29}$$

B.4. Upper boundary condition: litter (no pond)

The flux of the minor isotopologue into the top of the litter layer is:

$$q^i_s = c_{prec} q_{prec} - (c^i_{evap,out} q_{evap,out} - c^i_{evap,in} q_{evap,in}) \tag{B.30}$$

As for the case with no litter or pond, we use equations (B.26) and (B.27) to evaluate $c^i_{evap,out}$ and $c^i_{evap,in}$. In order to obtain $c^i_{l,s}$, which is required to evaluate $c^i_{evap,out}$, we write the equation for conservation of the minor isotopologue at the air/litter interface, which is analogous to Eq. (A.108):

$$\frac{\alpha_k}{r_{bw}}[c_{v,s} c^i_{l,s} \alpha^+(T_s) - c^i_{v,a}] = \alpha_{k,diff} \frac{D_{v,L}}{\Delta x_L/2}(c_{v,L}\alpha^+(T_L) c^i_{l,L} - c_{v,s} c^i_{l,s} \alpha^+(T_s)) \tag{B.31}$$

Rearranging Eq. (B.31) leads to the following expression for $c^i_{l,s}$:

$$c^i_{l,s} = \frac{\alpha_{k,diff} \frac{D_{v,L}}{\Delta x_L/2} c_{v,L} \alpha^+(T_L) c^i_{l,L} + c^i_{v,a} \alpha_k / r_{bw}}{\alpha^+(T_s)\alpha_k c_{v,s}/r_{bw} + \alpha^+(T_s)\alpha_{k,diff} c_{v,s} \frac{D_{v,L}}{\Delta x_L/2}} \tag{B.32}$$

The flux of the minor isotopologue from the litter layer to the soil column is:

$$q^i_0 = c_{prec} q_d - (c^i_{evap,out,L} q_{evap,out,L} - c^i_{evap,in,L} q_{evap,in,L}) \tag{B.33}$$

with

$$q_{evap,out,L} = \frac{D_{v,L}}{dx_L/2} c_{v,1} \tag{B.34}$$

$$c^i_{evap,out,L} = \alpha_k \alpha^+(T_0) c^i_{l,0} \tag{B.35}$$

and

$$q_{evap,in,L} = \frac{D_{v,L}}{dx_L/2} c_{v,L} \tag{B.36}$$

$$c^i_{evap,in,L} = \alpha_k c^i_{l,L}$$

The drainage flux, q_d (Eq. (A.68)) is the throughfall of precipitation, which occurs when rain falls on saturated litter, and is assumed to have the isotopic composition of the precipitation.

Similarly to Eq. (A.110), the equation for conservation of the minor isotopologue at the litter/soil interface is:

$$\begin{aligned} &\alpha_{k,diff} \frac{D_{v,L}}{\Delta x_L/2}\left[c_{v,0} c^i_{l,0} \alpha^+(T_0) - c_{v,L}\alpha^+(T_L) c^i_{l,L}\right] \\ &\quad = \alpha_{k,diff} \frac{D_{v,1}}{\Delta x_1/2}(c_{v,1}\alpha^+(T_1) c^i_{l,1} - c_{v,0} c^i_{l,0} \alpha^+(T_0)) - q_{l,0}(w_0 c^i_{l,0} + w_1 c^i_{l,1}) \\ &\qquad + \frac{D^i_{l,1}}{\Delta x_1/2}(c^i_{l,1} - c^i_{l,0}) \end{aligned} \tag{B.37}$$

Rearranging Eq. (B.37) leads to the following expression for $c^i_{l,0}$, which is required to evaluate $c^i_{evap,out,L}$:

$$c^i_{l,0} = \frac{\alpha_{k,diff} \frac{D_{v,1}}{\Delta x_1/2} c_{v,1} \alpha^+(T_1) c^i_{l,1} + \alpha_{k,diff} \frac{D_{v,L}}{\Delta x_L/2} c_{v,L} \alpha^+(T_L) c^i_{l,L} - q_{l,0} c^i_{l,1} w_1 + \frac{D^i_{l,1}}{\Delta x_1/2} c^i_{l,1}}{\alpha^+(T_0)\alpha_{k,diff} c_{v,0} \frac{D_{v,L}}{\Delta x_L/2} + q_{l,0} w_0 + \alpha^+(T_0)\alpha_{k,diff} c_{v,0} \frac{D_{v,1}}{\Delta x_1/2} + \frac{D^i_{l,1}}{\Delta x_1/2}} \tag{B.38}$$

B.5. Upper boundary condition: ponding

If a pond is present, it is assumed to be well-mixed. i.e. the concentration of the minor isotopologue at the pond surface is assumed equal to than in the bulk pond water: $c^i_{l,s} = c^i_{l,0}$. The flux of the minor isotopologue into the top of the pond is given by Eq. (B.30) with $c^i_{evap,in}$ given by Eq. (B.27) and $c^i_{evap,out}$ given by Eq. (B.26).

B.6. Lower boundary condition

The flux of the minor isotopologue at the lower boundary of the soil column is:

$$q^i_{w,n} = c^i_{l,n} q_{w,n} \tag{B.39}$$

B.7. Kinetic and Equilibrium fractionation factors

The liquid–vapour isotopic fractionation factor at equilibrium, α^+, was determined by Majoube (1971) as a function of T (K):

$$\alpha^+ = \exp\left(-\left[\frac{a}{T^2} + \frac{b}{T} + c\right]\right) \tag{B.40}$$

with coefficient values of $a = 24{,}844$; $b = -76.284$; $c = 0.052612$ for HDO and $a = 1137$; $b = -0.4156$; $c = -0.0020667$ for $H_2{}^{18}O$.

Vapour-phase kinetic fractionation factors require ratio of vapour-phase diffusion coefficients $\alpha_{k,diff} = D^i_v/D_v$. Merlivat et al.

(Merlivat, 1978) determined values of $\alpha_{k,diff} = 0.9755$ for HDO and $\alpha_{k,diff} = 0.9723$ for $H_2{}^{18}O$. These values were used in the Plausibility Test Cases and tests against analytical solutions (Sections 3.1, 3.2 and 3.3). Elsewhere, we use the newer measurements of Cappa et al. (2003), which are closer to the predictions of kinetic theory: $\alpha_{k,diff} = 0.9839$ for HDO and $\alpha_{k,diff} = 0.9691$ for $H_2{}^{18}O$. In contrast to Merlivat et al., Cappa et al. considered the effects of evaporative surface cooling, which explains the significant differences between the two sets of measurements. There are several formulations relating $\alpha_{k,diff}$ to α_k, the kinetic fractionation factor at the soil/air interface, and these are discussed in detail by Braud et al. (2005a). In this work, we used the formulation proposed by Mathieu and Bariac (1996):

$$\alpha_k = (\alpha_{k,diff})^{n_k} \tag{B.41}$$

with

$$n_k = \frac{(\theta_s - \theta_r)n_a + (\theta_{sat} - \theta_s)n_s}{(\theta_{sat} - \theta_r)} \tag{B.42}$$

where θ_s is the soil volumetric water content at the soil surface and coefficients n_a and n_s have respective values of 0.5 and 1.

Following Cuntz et al. (2007) the ratio of the liquid diffusivity of the minor isotopologue in $H_2O_{(l)}$ to the self diffusivity of $H_2O_{(l)}$ is $D_l^i/D_l = 1/1.013$ for HDO and $D_l^i/D_l = 1/1.026$ for $H_2{}^{18}O$. D_l depends on T (K) as:

$$D_l = 100 \cdot 10^{-9} \exp\left(-\frac{577}{T - 145}\right) \tag{B.43}$$

Appendix C. Root extraction

Root-water uptake was modelled as:

$$r_{ex}(\theta, z) = \alpha(\theta) g(z) q_{trans} \tag{C.1}$$

where $\alpha(\theta)$ is the root efficiency function of Lai and Katul (2000) and $g(z)$ is the vertical root density distribution of Li et al. (1999) The root efficiency function is defined by:

$$\alpha(\theta) = \min[1.0, \alpha_1(\theta) \times \alpha_2(\theta)] \tag{C.2}$$

Here $\alpha_1(\theta)$ is the maximum efficiency when soil moisture is not limiting root water uptake, defined as the maximum of local and non-local limits:

$$\alpha_1(\theta) = \max\left\{\frac{\theta}{\theta_s - \theta_w}; \frac{\int_0^z \theta(z)dz}{\int_0^L \theta(z)dz}\right\} \tag{C.3}$$

And $\alpha_2(\theta)$ is a root "shut-down" function:

$$\alpha_2(\theta) = \left(\frac{\theta - \theta_w}{\theta_s}\right)^{\gamma/(\theta - \theta_w)} \tag{C.4}$$

where γ is an empirical parameter controlling the rate at which $\alpha_2(\theta)$ approaches 0, which was set to 10^{-8} in this work.

The discrete version of the vertical root density distribution is expressed as the fraction of the root length density between depths z_i and z_{i+1}:

$$F_i = \frac{\ln[1 + e^{-bz_i}]/(1 + e^{-bz_{i+1}}) + 0.5(e^{-bz_i} - e^{-bz_{i+1}})}{\ln[2/(1 + e^{-bz_r})] + 0.5(1 - e^{-bz_r})} \tag{C.5}$$

where z_r is the rooting depth and b is an empirical root distribution parameter (Li et al., 2001):

$$b = \frac{24.66 F_{10}^{1.59}}{z_r} \tag{C.6}$$

and F_{10} is the fraction of root length density in the top 10% of the root zone. In this work we assumed values of $z_r = 10$ m and $F_{10} = 0.2$.

References

Barnes, C.J., Allison, G.B., 1983. The distribution of deuterium and ^{18}O in dry soils. 1. Theory. Journal of Hydrology 60 (1–4), 141–156.

Barnes, C.J., Allison, G.B., 1984. The distribution of deuterium and ^{18}O in dry soils. 3. Theory for non-isothermal water-movement. Journal of Hydrology 74 (1–2), 119–135.

Braud, I. et al., 2005b. SiSPAT-Isotope, a coupled heat, water and stable isotope (HDO and $H_2{}^{18}O$) transport model for bare soil. Part II. Evaluation and sensitivity tests using two laboratory data sets. Journal of Hydrology 309 (1–4), 301–320.

Braud, I. et al., 2009b. Isotopic composition of bare soil evaporated water vapor. Part I: RUBIC IV experimental setup and results. Journal of Hydrology 369 (1–2), 1–16.

Braud, I., Bariac, T., Gaudet, J.P., Vauclin, M., 2005a. SiSPAT-Isotope, a coupled heat, water and stable isotope (HDO and $H_2{}^{18}O$) transport model for bare soil. Part I. Model description and first verifications. Journal of Hydrology 309 (1–4), 277–300.

Braud, I., Bariac, T., Biron, P., Vauclin, M., 2009a. Isotopic composition of bare soil evaporated water vapor. Part II: modeling of RUBIC IV experimental results. Journal of Hydrology 369 (1–2), 17–29.

Brooks, R.H., Corey, A.T., 1964. Hydraulic Properties of Porous Media, vol. 3. Civil Engineering Department, Colorado State University, Fort Collins.

Campbell, G.S., 1974. Simple method for determining unsaturated conductivity from moisture retention data. Soil Science 117 (6), 311–314.

Campbell, G.S., 1985. Soil physics with basic. Transport models for soil–plant systems. Developments in Soil Science, vol. 14. Elsevier, Amsterdam. 150 pp.

Cappa, C.D., Hendricks, M.B., DePaolo, D.J., Cohen, R.C., 2003. Isotopic fractionation of water during evaporation. Journal of Geophysical Research – Atmospheres 108 (D16).

Cuntz, M., Ogee, J., Farquhar, G.D., Peylin, P., Cernusak, L.A., 2007. Modelling advection and diffusion of water isotopologues in leaves. Plant Cell and Environment 30 (8), 892–909.

De Vries, D.A., 1975. Heat transfer in soils. In: De Vries, D.A., Afgan, N.H. (Eds.), Heat and Mass Transfer in the Biosphere. John Wiley and Sons, pp. 5–28.

Dole, M., Lane, G.A., Runn, D.P., Zaukelies, D.A., 1954. Isotopic composition of atmospheric oxygen and nitrogen. Geochimica Et Cosmochimica Acta 6 (2–3), 65–78.

Feddes, R.A. et al., 2001. Modeling root water uptake in hydrological and climate models. Bulletin of the American Meteorological Society 82 (12), 2797–2809.

Fekete, B.M., Gibson, J.J., Aggarwal, P., Vorosmarty, C.J., 2006. Application of isotope tracers in continental scale hydrological modeling. Journal of Hydrology 330 (3–4), 444–456.

Ferretti, D.F. et al., 2003. Partitioning evapotranspiration fluxes from a Colorado grassland using stable isotopes: seasonal variations and ecosystem implications of elevated atmospheric CO2. Plant and Soil 254 (2), 291–303.

Gonfiantini, R., 1978. Standards for stable isotope measurements in natural compounds. Nature 271 (5645), 534–536.

Gonzalez-Sosa, E., Braud, I., Thony, J.L., Vauclin, M., Calvet, J.C., 2001. Heat and water exchanges of fallow land covered with a plant-residue mulch layer: a modelling study using the three year MUREX data set. Journal of Hydrology 244 (3–4), 119–136.

Ham, J.M., 2005. Useful equations and tables in micrometeorology. In: Viney, M.K. (Ed.), Micrometeorology in agricultural systems, Agronomy. CSIRO Marine and Atmospheric Research paper. Report No. 013. American Society of Agronomy, Inc., Madison, Wisconsin, pp. 533-560.

Haverd, V., Leuning, R., Griffith, D.W.T., Van Gorsel, E., Cuntz, M., 2009. The turbulent Lagrangian time scale in forest canopies constrained by fluxes, concentrations and source distributions. Boundary-Layer Meteorology 130, 209–228.

Henderson-Sellers, A. et al., 2006. Stable water isotope simulation by current land-surface schemes: results of iPILPS phase 1. Global and Planetary Change 51 (1–2), 34–58.

Hoffmann, G. et al., 2004. A model of the Earth's Dole Effect. Global Biogeochemical Cycles 18 (1), GB1008.

Jouzel, J. et al., 2007. Orbital and millennial Antarctic climate variability over the past 800,000 years. Science 317 (5839), 793–796.

Kowalczyk, E.A. et al., 2006. The CSIRO Atmosphere Biosphere Land Exchange (CABLE) model for use in climate models and as an offline model. 013.

Lai, C.T., Katul, G., 2000. The dynamic role of root-water uptake in coupling potential to actual transpiration. Advances in Water Resources 23, 427–439.

Leuning, R., Cleugh, H.A., Zegelin, S.J., Hughes, D., 2005. Carbon and water fluxes over a temperate Eucalyptus forest and a tropical wet/dry savanna in Australia: measurements and comparison with MODIS remote sensing estimates. Agricultural and Forest Meteorology 129 (3–4), 151–173.

Li, K.Y., Boisvert, J.B., De Jong, R., 1999. An exponential root-water-uptake-model Canadian. Journal of Soil Science 79, 333–343.

Li, K.Y., De Jong, R., Boisvert, J.B., 2001. An exponential root-water-uptake model with water stress compensation. Journal of Hydrology 252, 189–204.

Majoube, M., 1971. Oxygen-18 and deuterium fractionation between water and steam. Journal De Chimie Physique Et De Physico-Chimie Biologique 68 (10), 1423.

Mathieu, R., Bariac, T., 1996. A numerical model for the simulation of stable isotope profiles in drying soils. Journal of Geophysical Research – Atmospheres 101 (D7), 12685–12696.

Matthews, S., 2005. The water vapour conductance of Eucalyptus litter layers. Agricultural and Forest Meteorology 135 (1–4), 73–81.
Matthews, S., 2006. A process-based model of fine fuel moisture. International Journal of Wildland Fire 15 (2), 155–168.
McKenzie, N.J., Hook, J., 1992. Interpretation of the Atlas of Australian Soils. Technical Report 94/1992, CSIRO Division of Soils, Canberra.
Melayah, A., Bruckler, L., Bariac, T., 1996. Modeling the transport of water stable isotopes in unsaturated sails under natural conditions. 1. Theory. Water Resources Research 32 (7), 2047–2054.
Merlivat, L., 1978. Dependence of bulk evaporation coefficients on air–water interfacial conditions as determined by isotopic method. Journal of Geophysical Research – Oceans and Atmospheres 83 (NC6), 2977–2980.
Myrold, D.D., Elliott, L.F., Papendick, R.I., Campbell, G.S., 1981. Water potential-water content characteristics of wheat straw. Soil Science Society of America Journal 45, 329–333.
Ogée, J. et al., 2004. Partitioning net ecosystem carbon exchange into net assimilation and respiration with canopy-scale isotopic measurements: an error propagation analysis with $^{13}CO_2$ and $CO^{18}O$ data. Global Biogeochemical Cycles 18 (2).
Ogée, J., Brunet, Y., 2002. A forest floor model for heat and moisture including a litter layer. Journal of Hydrology 255 (1–4), 212–233.
Philip, J.R., 1957. Evaporation, and Moisture and Heat Fields in the Soil. Journal of Meteorology 14 (4), 354–366.
Riley, W.J., Still, C.J., Torn, M.S., Berry, J.A., 2002. A mechanistic model of $H_2{}^{18}O$ and $C^{18}OO$ fluxes between ecosystems and the atmosphere: model description and sensitivity analyses. Global Biogeochemical Cycles 16 (4).
Ross, P.J., 2003. Modeling soil water and solute transport – fast, simplified numerical solutions. Agronomy Journal 95 (6), 1352–1361.
Shurbaji, A.R.M., Phillips, F.M., 1995. A numerical-model for the movement of H_2O, $H_2{}^{18}O$, and ^2HHO in the unsaturated zone. Journal of Hydrology 171 (1–2), 125–142.
Wang, Y.P., Leuning, R., 1998. A two-leaf model for canopy conductance, photosynthesis and partitioning of available energy I: model description and comparison with a multi-layered model. Agricultural and Forest Meteorology 91 (1–2), 89–111.
Yoshimura, K., Miyazaki, S., Kanae, S., Oki, T., 2006. Iso-MATSIRO, a land surface model that incorporates stable water isotopes. Global and Planetary Change 51 (1–2), 90–107.